Geoscience Letters

RESEARCH LETTER

Open Access

Idealized simulations of tropical cyclones with thermodynamic conditions under reanalysis and CMIP5 scenarios

Cheng-Hsiang Chih[1], Kun-Hsuan Chou[2] and Chun-Chieh Wu[1,3*]

Abstract

The idealized Weather Research and Forecasting (WRF) simulations are conducted to investigate tropical cyclone (TC) size and intensity over the Western North Pacific (WNP) over the past decades, as represented by National Centers for Environmental Prediction/National Center for Atmospheric Research (NCEP/NCAR) R-1, European Center for Medium range Weather Forecasting (ECMWF) twentieth century (ERA20C) reanalysis, and National Oceanic and Atmospheric Administration Cooperative Institute for Research in Environmental Sciences 20th Century (CIRES20) Reanalysis V2 data, and under a future climate, as predicted by the Coupled Model Intercomparison Project Phase 5 (CMIP5). Firstly, sensitivity experiments with varying environmental thermodynamic forcing are conducted to examine how thermodynamic conditions affect TC size and intensity. Secondly, distributions of thermodynamic quantities taken from the NCEP/NCAR R-1, ERA20C, CIRES20, and CMIP5 data are used to initialize four more sets of WRF simulations. There is no significant variation in TC size nor intensity over the WNP within the past 90 years based on the idealized downscaling high-resolution WRF model, whereas those simulations initialized based on CMIP5 data show that both the TC size and intensity would increase in the future (2071–2100) of the representative concentration pathway 8.5 (RCP8.5) as compared to those during the current (2010–2040) climate stage of RCP8.5. An explanation for these findings is given by referring to impact of the air–sea thermal disequilibrium and acutely increasing temperature in the TC outflow, while their relation to previous works is also discussed.

Keywords: Tropical cyclone size, Climate change, Downscaling, Idealized simulation, Thermodynamic conditions

Introduction

In recent years, many previous studies have focused on the positive correlation between the size of tropical cyclones (TCs) and the severity of the ensuing disasters. Indeed, TC size is critical in determining the height of the storm surge, the extent of coastal flooding, and the area affected by landfall (Harris 1963; Irish et al. 2008; Grinsted et al. 2012). Moreover, it is well known that the large TCs tend to be accompanied by stronger environmental flow and heavy rainfall (Lander 1994; Liu and Chan 2002; Lee et al. 2010; Chih et al. 2015). As a case in point, Typhoon Morakot (2009) produced tremendous rainfall over Taiwan (with a maximum accumulated rainfall of 1623.5 mm in 24 h), yet with a mere peak intensity of 40 m s^{-1} (from Central Weather Bureau, Taiwan) corresponding to category 1 to 2 on the Saffir–Simpson Hurricane Scale, as discussed in a number of previous studies (Huang et al. 2011; Nguyen and Chen 2011; Yen et al. 2011; Wu 2013). Kun-Hsuan et al. (2011) demonstrated the large TC size of Morakot using radar reflectivity data from Central Weather Bureau (CWB) and microwave imagery from the Navy Research Laboratory's Tropical Cyclone Webpage as compared to many TCs. Although there is no direct evidence that could link the extreme events such as Morakot to global warming, it should be

*Correspondence: cwu@as.ntu.edu.tw

[1] Department of Atmospheric Sciences, National Taiwan University, No. 1, Sec. 4, Roosevelt Rd, Taipei 10617, Taiwan
Full list of author information is available at the end of the article

useful to examine the mechanisms affecting changes in TC size under the changing (warming) climate.

Several previous studies mentioned that the TC size is affected by thermodynamic factors (Emanuel 1986; Hill and Lackmann 2009; Khairoutdinov and Emanuel 2013; Chavas and Emanuel 2014; Stovern and Ritchie 2016). Emanuel (1986) indicated that the TC size (outer radius) will increase with increased sea surface temperature (T_{SST}), and with decreased outflow temperature (T_{out}). Hill and Lackmann (2009) indicated that the TC size is sensitive to the environmental humidity. The higher environmental humidity enhances generation of diabatic potential vorticity (PV) in spiral bands, which could further enhance upward latent heat and moisture flux that serve as positive feedback. Recently, Stovern and Ritchie (2016) suggested that the cooler atmospheric temperature will reduce the environmental humidity and the convective available potential energy (CAPE), but will enhance the sea surface heat fluxes (SSHF). The above impacts on TC size could be related to the global climate change. How anthropogenic warming will influence TC size is becoming an important scientific topic. Although many studies have discussed the possible dynamic mechanisms, they are out of the scope and will not be discussed in this study.

Different measures of TC size coexist in various literatures, such as the radius of the outermost closed isobar (ROCI) or the surface azimuthally averaged radius of some threshold wind speed, with 34 kt (R34) or 30 kt (R30) often chosen to represent the gale-force winds or outer-core TC size (Merrill 1984; Liu and Chan 1999; Kimball and Mulekar 2004; Yuan et al. 2007; Lee et al. 2010). R30 was shown to be highly correlated with the outer-core strength parameter as measured by aircraft observations (Weatherford and Gray 1988a, b). R64 generally represents the inner-core size (Weatherford and Gray 1988a). Therefore, both R30 and R64 (64 Knots, hurricane-force winds) of the 10-m wind speeds are utilized for analyzing the TC size in all experiments, which is consistent with previous studies. However, as discussed in Cocks and Gray (2002), a specific definition of TC size is critical because different definitions of TC size may lead to qualitatively different results (Merrill 1984; Liu and Chan 2002; Dean et al. 2009; Xu and Wang 2010a, b). In other words, the different TC size metrics may represent different parts of TCs.

Notwithstanding this ambiguity, understanding the factors determining TC size and its variation in relation to time of year, TC lifetime, ocean basin, geographic location, and track, remains an interesting and challenging research topic. In recent years, the climatology of TC size in the Western North Pacific (WNP) was shown in Knaff et al. (2014), indicating the non-statistically significant trends of increasing TC size based on storm-centered infrared imagery in the WNP. Previous studies of TC size using satellite scatterometer data have been successfully carried out, such as that by Chavas and Emanuel (2010), Chan and Chan (2012), and Chavas et al. (2016) who used QuikSCAT data from 1999 to 2008 to analyze TC climatology and the evolution of TC size over its life cycle. Chavas and Emanuel (2010) indicated that the spatial extent of a given TC remains relatively constant throughout its lifetime without external environmental forcing. Chan and Chan (2012) also identified characteristics of TC size in relation to the track, lifetime, and subtropical ridge activity. Furthermore, they indicated larger size and higher strength during El Niño and the contrary during La Niña based on the El Niño-Southern Oscillation (ENSO) index. After that, Chavas et al. (2016) further analyzed the statistical distributions of TC size and environmental parameters, and found a positive relationship between T_{SST} and TC size. However, we think the data in such rather short period are insufficient for analyzing warming climate-related impacts on TC size beyond a decadal scale.

To date, there are a few papers related to the changes in TC size under the future climate change. Lin and Emanuel (2016) indicated that the TC size under the impact of climate change still needs to be investigated through both observational and numerical studies. Nevertheless, Kim et al. (2014) showed that the global average increase in R30 is about 2.4% in the double CO_2 scenario by Geophysical Fluid Dynamics Laboratory Climate Model version 2.5 (GFDL-CM2.5). Knutson et al. (2015) also discussed the effect of a future warming climate on TC size based on downscaled framework simulations, showing that the TC size remains nearly constant globally but is decreased by about 8% in the WNP, indicating substantial inter-basin variability. However, they did not investigate the influence of possible factors affecting the TC size under future climate conditions. Yohei et al. (2017) also showed that the TC size defined by a radius of 12 ms^{-1} surface wind is projected to increase in the WNP using global nonhydrostatic model under Emissions Scenarios (SRES) A1B of the phase-3 World Climate Research Program (WCRP), the Coupled Model Intercomparison Project (CMIP3; Meehl et al. 2007).

Therefore, the purpose of this paper is to investigate possible changes of TC size and intensity under different climate thermodynamic conditions and to illustrate how air–sea thermal disequilibrium affects TC size based on idealized Weather Research and Forecasting (WRF) model simulations in the WNP. TC size is investigated here mainly to allow for an internal consistency check as compared to other studies. We first determine whether the vortex intensity of simulations is consistent with the

previous studies. In recent years, studies on TC climatology mostly focus on intensity, track, frequency, or number (Chan 1985, 2000; Chia and Ropelewski 2002; Wang and Chan 2002; Matsuura et al. 2003; Ho et al. 2004, 2006; Webster et al. 2005; Wu et al. 2005; Tu et al. 2009; Knutson et al. 2010, 2015, 2020). The extant TC intensity studies showed mixed results based on different analysis methods. For instance, Emanuel (2005) proposed the calculation of the Power Dissipation Index (PDI) based on the cube-time integral of the TC's maximum surface wind speed (MWS), and found that the PDI has had an obvious upward trend since the 1970s. However, Klotzbach (2006) used the cyclone energy index (Accumulated cyclone energy, ACE) to calculate the square of the TC's MWS over time and analyzed different ocean surfaces, but obtained different results from that in Emanuel (2005). From the climate perspective, most research showed that the TC intensity tends to increase in WNP and Atlantic (ALT) under the future climate scenarios. Recently, Gutmann et al. (2018) examined TC intensity, precipitation rate, translation speed, size, and Cyclone Damage Potential (CDP) utilized by pseudo-global warming, indicating that both the intensity and CDP are increasing in the warmer future. However, few studies have low-to-medium confidence in this result of TC intensity change in WNP (Hasegawa and Emori 2007; Oouchi et al. 2006; Kim et al. 2014; Knutson et al. 2015). To clarify the issues discussed above, four sets of sensitivity experiments are conducted in high horizontal grid resolution (5 km) and are used to analyze the relations among size, intensity, and SSHF of a TC. Environmental thermodynamic conditions including T_{SST}, atmospheric temperature (T_{atm}), and relative humidity (RH) in the WNP are taken from National Centers for Environmental Prediction/National Center for Atmospheric Research (NCEP/NCAR) R-1 reanalysis data (Kalnay et al. 1996), European Center for Medium range Weather Forecasting (ECMWF) twentieth century (ERA20C) reanalysis (Poli et al. 2016), and National Oceanic and Atmospheric Administration (NOAA) Cooperative Institute for Research in Environmental Sciences 20th Century (CIRES20) Reanalysis V2 (Compo et al. 2011), and are used as the model initial conditions to investigate the TC size evolution within the past 90 years. In addition, the Coupled Model Intercomparison Project Phase 5 (CMIP5, Taylor et al. 2012) data are used to perform model simulations under the Representative Concentration Pathways 4.5 (RCP4.5) and RCP8.5 scenarios in order to assess the impact of climate change-induced thermodynamic forcing on TC size and intensity in particular. This paper is organized as follows: "Model and experimental design" section presents the model and experimental design. "Results" section describes the model results. Discussion and "Conclusions" sections presents our conclusions and discusses the relevance thereof in the context of previous works.

Model and experimental design

Model

The Weather Research and Forecast model (WRF-em_tropical cyclone) version 4.0 is used here to simulate the storm evolution under idealized thermodynamic conditions, starting from an identical idealized incipient vortex (Skamarock et al. 2008). To eliminate the nonlinear effects of environmental dynamic forcing, the background wind field is set to zero (i.e., no steering flow, no topography effect, and no vertical wind shear). Sixty-five vertical layers with eta level coordinates are utilized in the model simulations, and the reference model top is 25 km. The incipient, symmetric and baroclinic vortex is adopted from the analytical formula of Rotunno and Emanuel (1987) in a quiescent environment, with the initial outer radius set at 412.5 km and the initial radius of maximum wind at 82.5 km. To reduce computation time for simulating the early development, the initial maximum tangential wind at the lowest level is set at 25 m s^{-1}. No cumulus parameterization scheme is used in any of the simulations. The Thompson scheme is used for the parameterization of microphysical processes (Thompson et al. 2008). The Rapid Radiative Transfer Model for General circulation models (RRTMG) scheme is used to estimate the effects of longwave and shortwave radiations (Iacono et al. 2008; RRTMG). The Yonsei University (YSU) schemes (Hong et al. 2006) and the Revised MM5 Monin–Obukhov scheme (Jimenez et al. 2012) are used for the planetary boundary layer and surface layer, respectively. A single squared 2000 km × 2000 km domain is configured as large as possible for reducing the effect of doubled periodic lateral boundary condition. The model grid spacing in the horizontal is 5 km. The sponge layer is 5 km from the model top. In addition, the initial moist-neutral horizontally homogeneous environmental sounding profile of Jordan (1958) is used in the sensitivity experiments. A number of the simulations have been tested by different combined schemes including physics, dynamics schemes, initial vortexes, and lateral boundaries (see Additional file 1: Fig. S1). All the simulations use the same incipient vortex design and model schemes.

Several previous studies indicated the positive correlation between the latitude and size of TCs (DeMaria and Pickle 1988; Li et al. 2012; Chan and Chan 2014). According to Radu et al. (2014), the intensity of hurricane Katrina increased by about 20% in their experiments when T_{SST} and T_{atm} was increased uniformly by 2 °C. However, the track differences and vertical wind shear that

were allowed in their experiments may affect the tropical cyclone structure (Zhang and Tao 2013; He et al. 2015). Therefore, all simulations are performed on an f-plane (20° latitude) to eliminate the impacts of the track errors/Coriolis force on TC size in our study.

The results indicate that the vortex would achieve a quasi-steady-state of TC intensity with very small fluctuation after about 96 h. However, the intensity tends to remain consistent across simulations with different T_{SST} after around 432 h (see Additional file 1: Fig. S1). The quasi-steady-state of TC associated with the intensity change has also been examined by Hakim (2011) and Chavas and Emanuel (2014) who mentioned that the time scales of equilibrium state are longer than the real TC lifespan (30 days in their simulations), and it is difficult to reach a truly quasi-steady-state in real TCs. Hill and Lackmann (2009) also showed that the TC size may continue to grow slowly under the favorable environmental conditions with quasi-steady intensity after 240 h of the simulations. In this study, changes in intensity and radius of maximum wind (not shown) across simulations are relatively small with some fluctuations from the integrated time 96 to 144 h, which is called "locally steady" by Hakim (2011). Despite failing to reach a perfectly steady state, the TC lifespan of the following simulations is reasonable for general analyses. Therefore, the statistical test period is chosen from 96 to 144 h, excluding the spin-up time at the beginning of simulation. To determine the effective degrees of freedom for our simulations in the following analyses by referring to Davis (1976), Chen (1982), and Zhao and Li (2009), we first need to take into account prevention of overconfident results. Meanwhile, to avoid assumptions of normal distribution and the dependent data problem, a two-tailed moving-blocks bootstrap-based test with 10,000 resamples and a two-sample z-test are employed in the mature period to verify if the differences in TC intensity and size (R30 and R64) among different experiments are statistically significant. The confidence level is over 99% with an effective degree of freedom at around 10, which can be referred to as "significant". Moreover, the Cohen's ***d*** effect size (Cohen 1988) of each variable by subtracting the mean of two samples and then dividing the value by the standard deviation of the two conditions represents the relative strength of the relationship between the two variables in this study.

In addition to T_{SST}, T_{atm}, water vapor mixing ratio (r_v) and carbon dioxide (CO_2) concentration, SSHF is also a useful parameter for analysis, as described below. The diagnostics of SSHF and r_v are averaged within 300 km of the storm center in the present work (Table 4). SSHF can be inferred from a bulk aerodynamic formula. According to Liu et al. (1979),

$$\mathrm{SSHF} = \rho C_p \overline{w'\theta'} + \rho L_v \overline{w'q'}, \quad (1)$$

$$\overline{w'\theta'} = C_H |U| (\theta_s - \theta),$$

$$\overline{w'q'} = C_Q |U| A_m (q_s - q),$$

where ρ is the density of air, C_p is the specific heat of air at constant pressure, w is vertical wind speeds, θ_s and θ are the sea surface and near-surface atmospheric potential temperature, respectively, w', θ' and q' are the instantaneous fluctuations of vertical wind velocity, temperature and specific humidity, respectively, L_v is the latent heat of the vaporization of water, and C_H is the exchange coefficient of sensible heat. C_Q is the exchange coefficient of latent heat. U is the average value of the wind speed relative to the sea surface at the height of 10 m, A_m is the moisture availability from the sea surface, which is set to 1 since the idealized TC simulations are located over water without topography, while q_s and q are the sea surface and near-surface atmospheric specific humidity, respectively. Note that the term containing L_v (latent heat flux) is typically dominant over the C_p term (sensible heat flux) on the right-hand side of Eq. (1). The above equations are also applied in WRF simulations.

Our idealized experiments provide high-resolution simulations to investigate how TC size is related to T_{SST}, T_{atm}, r_v and CO_2 concentration which is controlled by radiative schemes under different climate conditions. Notably, since the sounding file format of WRF is r_v, in this study the RH is converted to r_v from the reanalysis data (Bolton 1980).

Experimental design

Sensitivity experiments

Four sets of sensitivity experiments with different T_{SST}s, T_{atm}s, r_v s, and CO_2s concentrations are performed: (1) the S-SST experiments whose T_{SST} varies from 28.0 °C to 32.0 °C in steps of 1.0 °C (S-SST28, S-SST29, CTL, S-SST31, and S-SST32, respectively) remain constant in the whole domain and each simulation as in Nolan et al. (2007) and Emanuel et al. (2014). (2) The S-AT experiment whose T_{atm} of the entire vertical profile is modified uniformly at the initial time by ± 2.0 °C of CTL (S-AT-2; S-AT + 2) without changing T_{SST}, r_v and CO_2 concentration. (3) The S-MR experiment whose r_v of the entire vertical profile is modified uniformly at the initial time by ± 10.0% of CTL (S-MR-10; S-MR + 10) without changing T_{SST}, T_{atm}, and CO_2 concentration. The RH of S-MR experiments does not exceed 100% over time. (4) The S-CO_2 experiment whose atmospheric CO_2 concentration is doubled (S-CO_2 × 2, 758 ppm) or quadrupled (S-CO_2 × 4, 1516 ppm) by CTL without changing T_{SST},

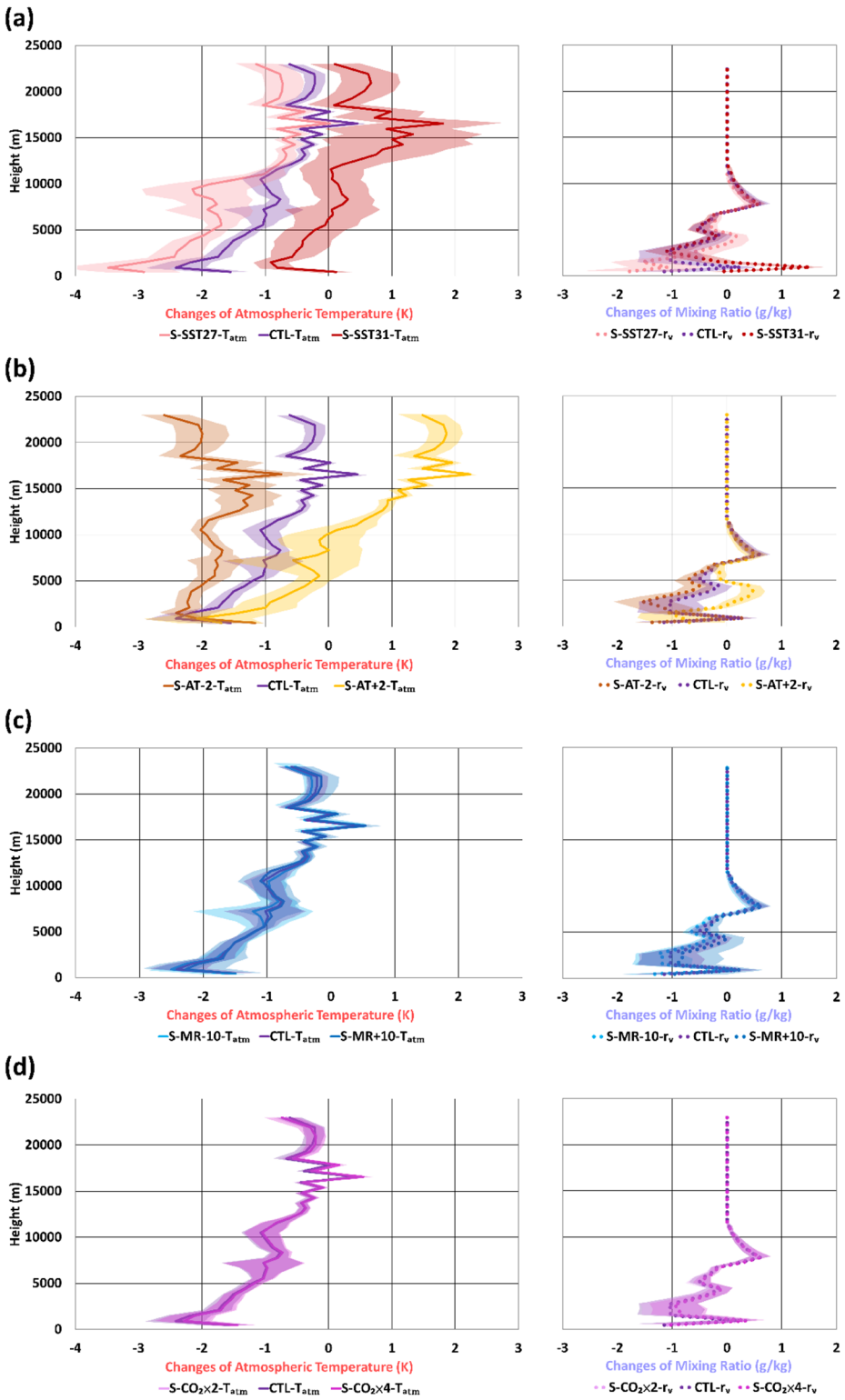

Fig. 1 The mean state (bold line) and standard deviation (shaded) from 0 to 336 h in azimuthal average at 1000 km distance from the TC center for vertical profile of T_{atm} and r_V in the following sensitivity experiments: **a** S-SST, **b** S-AT, **c** S-MR, and **d** S-CO2, are calculated as differences from the Jordan (1958) sounding profile

T_{atm}, and r_v. The CO_2 concentration will reach 758 (1516) ppm around year 2080 (2159) under RCP8.5 by CMIP5. Although the simplified sensitivity experiments are not realistic, the thermodynamic mechanisms can be investigated by performing these simulations. To isolate the cause and effect of these experiments, the mean state and its standard deviation of the environmental sounding in the region outside of the vortex center from 1900 to 2000 km and from 0 to 144 h are plotted in Fig. 1. The pattern is similar to the time period from 96 to 144 h (not shown). Due to the systematic difference of T_{atm} and r_v as shown in the S-SST and S-AT experiments (Fig. 1a, b), the subsequent analysis of the different TC responses across experiments can be reasonably attributed to the externally imposed thermodynamic changes. In addition, although changing r_v of the boundary layer air is directly modifying the air–sea thermodynamic disequilibrium, Fig. 1c shows a similar pattern in S-MR for T_{atm} and r_v. The process is analogous to S-CO_2 in Fig. 1d, which implies the radiative forcing of CO_2 might be quite small.

Reanalysis experiments

Environmental thermodynamic conditions in the past decades are taken from the reanalysis dataset and used as initial conditions for another set of experiments. The NCEP/NCAR R-1 reanalysis, ECMWF twentieth century reanalysis, and NOAA CIRES 20th Century reanalysis V2 data contain monthly mean vertical profiles from July to September of 1951 to 2010, 1921 to 2010, and 1921 to 2010, respectively. The data cover an area representing WNP from 5° to 30° N, and 130° to 180° E, which refers to the definition of WNP region by Chan and Liu (2004) but excluding the area of Taiwan and Philippines topography from 5° to 30° N, and 120° to 130° E. Note that several previous studies mentioned that the uncertainty may be affected by many factors such as the change in observation and model systems for reanalysis data (Thorne and Vose 2010; Parker 2016). Although Vecchi et al. (2013) also suggested that the long-term trend of NCEP/NCAR R-1 cannot be accurately assessed for tropical temperature changes in the upper troposphere, it is still valuable to investigate the differences of reanalysis data as a reference. To satisfy the standard averaging period for climate studies (30 years), we divide the datasets into three stages: pre-stage (1921–1950, P), mid-stage (1951–1980, M), and later-stage (1981–2010, L). The initial conditions including T_{atm}, T_{SST}, r_v, surface of r_v, sea level pressure and geopotential height are computed by spatial and temporal (from July to September) averaging at each stage and are used to initialize each experiment. Meanwhile, the average CO_2 concentration of these three stages is taken from Meinshausen et al. (2011) using the reduced-complexity carbon cycle climate Model for the Assessment of Greenhouse Gas Induced Climate Change version 6 (MAGICC6). A summary of the reanalysis data change is shown in Fig. 2. The results show that the greatest warming in the upper troposphere (near the 100 to 200 hPa level) and the greatest moistening in the mid-lower troposphere (near the 1000 to 600 hPa level) between pre-stage and later-stage is found in ERA20C (Fig. 2b, c). Note that the T_{atm} in the upper troposphere of NCEP and

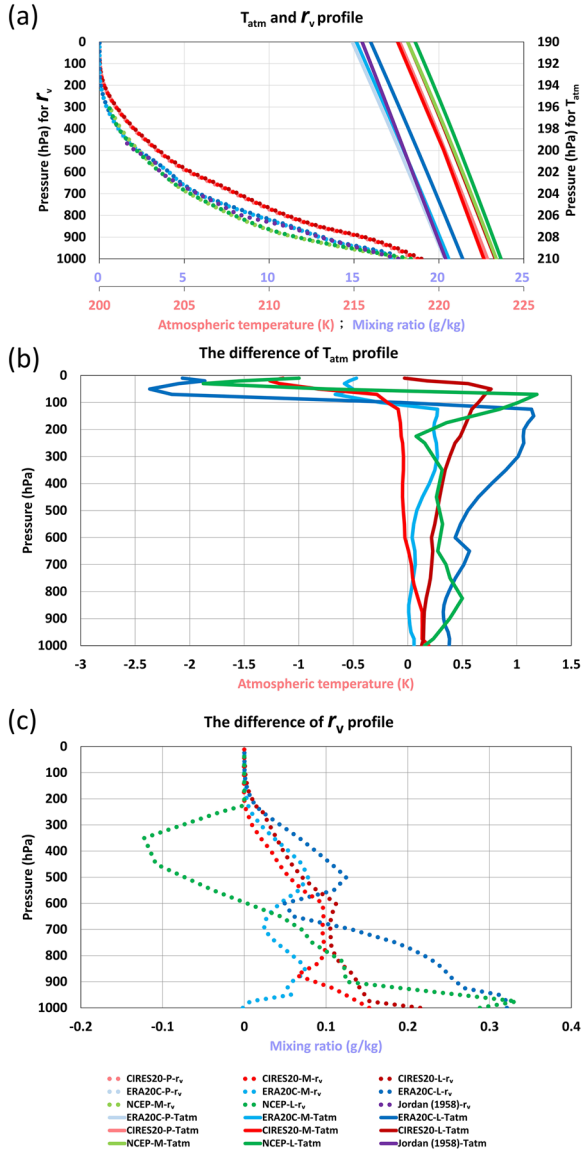

Fig. 2 **a** The spatially and temporally averaged vertical profiles of T_{atm} (solid lines) in the upper troposphere and r_v (dashed lines) for the following reanalysis data: NCEP/NCAR R-1 (green), ERA20C (blue), and CIRES20 (red) and the vertical profile of Jordan (1958) sounding (purple). P is pre-stage from 1921 to 1950, M is mid-stage from 1951 to 1981, and L is later-stage from 1981 to 2010. **b** The changes of T_{atm} and **c** r_v were calculated as differences between pre-stage and other stages of reanalysis experiments, but differences between mid-stage and later-stage were calculated for NCEP/NCAR R-1

Table 1 The sensitivity, reanalysis and CMIP5 experiments with values of design variables

Experiments	$CO_{2\ (ppm)}$	T_{SST} (°C)	T_{SST}—near-surface T_{atm} (°C)	r_v	T_{atm}
CTL	379	30.0	4.0	Jordan (1958)	Jordan (1958)
S-CO_2	758 ($CO_2 \times 2$)	30.0	4.0	Jordan (1958)	Jordan (1958)
	1516 ($CO_2 \times 4$)		4.0		
S-SST	379	28.0	2.0	Jordan (1958)	Jordan (1958)
		29.0	3.0		
		31.0	5.0		
		32.0	6.0		
S-MR	379	30.0	4.0	Jordan (1958) − 10.0%	Jordan (1958)
			4.0	Jordan (1958) + 10.0%	
S-AT	379	30.0	6.0	Jordan (1958)	Jordan (1958) − 2.0 °C
			2.0		Jordan (1958) + 2.0 °C
NCEP-M	321	28.6	0.9	NCEP-M-r_v	NCEP-M-T_{atm}
NCEP-L	362	28.8	1.0	NCEP-L-r_v	NCEP-L-T_{atm}
CIRES20-P	308	28.4	1.7	CIRES20-P-r_v	CIRES20-P-T_{atm}
CIRES20-M	321	28.5	1.7	CIRES20-M-r_v	CIRES20-M-T_{atm}
CIRES20-L	362	28.7	1.7	CIRES20-L-r_v	CIRES20-L-T_{atm}
ERA20C-P	308	28.4	3.5	ERA20C-P-r_v	ERA20C-P-T_{atm}
ERA20C-M	321	28.6	3.6	ERA20C-M-r_v	ERA20C-M-T_{atm}
ERA20C-L	362	28.7	3.4	ERA20C-L-r_v	ERA20C-L-T_{atm}
RCP4.5-C	424	28.6	2.1	RCP4.5-C-r_v	RCP4.5-C-T_{atm}
RCP4.5-F	532	29.5	2.1	RCP4.5-F-r_v	RCP4.5-F-T_{atm}
RCP8.5-C	435	28.7	2.1	RCP8.5-C-r_v	RCP8.5-C-T_{atm}
RCP8.5-F	807	30.8	1.9	RCP8.5-F-r_v	RCP8.5-F-T_{atm}

The profiles of T_{atm} and r_v are shown in Fig. 2

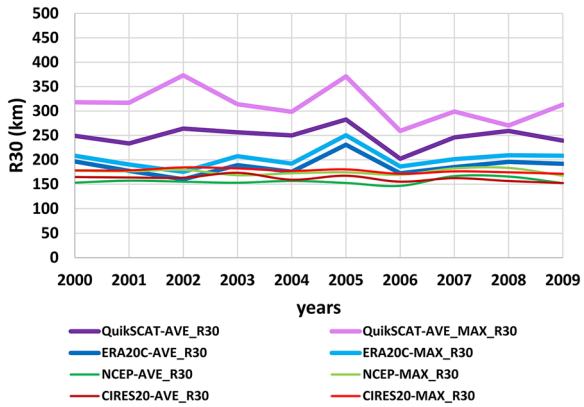

Fig. 3 The average R30 (Dark purple) and average maximum R30 (Light purple) of QuikSCAT and reanalysis experiments for NCEP (Green), ERA20C (Blue), and CIRES20 (Red) from 2000 to 2009, respectively

CIRES20 are greater than those of ERA20C (Fig. 2a), and the difference between the near-surface T_{atm} and T_{SST} in ERA20C is greater than those in CIRES20 and NCEP (Table 1). To verify whether the idealized WRF model simulations are close to observation, we conduct simulations using annual mean data from July to September under the same methodology and variables (T_{atm}, T_{SST}, r_v, surface of r_v, sea level pressure and geopotential height) as in the above three reanalysis experiments from 2000 to 2009 (with 30 simulations in total), and compare them to R30 of QuikSCAT, the information of which is taken from a remote sensing system (RSS), including the average R30 of TC lifespan and the average maximum R30 of each TC per year (Fig. 3). The result shows that the experiments of ERA20C is consistent with the tendency of observational TC size, which can be expected to improve confidence for the results of long-term TC size changes in the past.

Table 2 The case number of TCs for QuickSCAT data in the WNP from 2000 to 2009

Year	2000	2001	2002	2003	2004	2005	2006	2007	2008	2009
Case number	8	7	6	5	7	11	7	5	3	5

Table 3 Information for the CMIP5 dataset included in the CMIP5 experiments

Model	Institution
ACCESS1.0	CSIRO (Commonwealth Scientific and Industrial Research Organisation, Australia), and BOM (Bureau of Meteorology, Australia)
ACCESS1.3	
BNU-ESM	BNU (Beijing Normal University)
CanESM2	CCCma (Canadian Centre for Climate Modelling and Analysis)
CCSM4	NCAR (National Center for Atmospheric Research)
CESM1-BGC	NSF (National Science Foundation), Department of Energy, National Center for Atmospheric Research
CESM1-CAM5	
CNRM-CM5	Centre National de Recherches Météorologiques / Centre Européen de Recherche et de Formation Avancée en Calcul Scientifique
CNRM-ESM1	
CSIRO-Mk3.6.0	Commonwealth Scientific and Industrial Research Organisation in collaboration with the Queensland Climate Change Centre of Excellence
FGOALS-g2	LASG, Institute of Atmospheric Physics, Chinese Academy of Sciences; and CESS, Tsinghua University
FGOALS-s2	LASG, Institute of Atmospheric Physics, Chinese Academy of Sciences
FIO-ESM	The First Institute of Oceanography, SOA, China
GFDL-CM3	GFDL (Geophysical Fluid Dynamics Laboratory)
GFDL-ESM2G	
GFDL-ESM2M	
HadGEM2-EC	Met Office Hadley Centre (additional HadGEM2-ES realizations contributed by Instituto Nacional de Pesquisas Espaciais)
INM-CM4	INM (Institute for Numerical Mathematics)
IPSL-CM5A-LR	IPSL (Institut Pierre-Simon Laplace)
IPSL-CM5A-MR	
IPSL-CM5B-LR	
MIROC5	Atmosphere and Ocean Research Institute (The University of Tokyo), National Institute for Environmental Studies, and Japan Agency for Marine-Earth Science and Technology
MIROC-ESM	
MIROC-ESM-CHEM	
MRI-CGCM3	MRI (Meteorological Research Institute)
NorESM1-ME	NCC (Norwegian Climate Centre)

The number of TCs per year is shown in Table 2. Note that the QuickSCAT cannot cover all TCs every year, and the absolute values of R30 are not meaningful for this comparison. This is also consistent with Schenkel et al. (2017), who showed that the reanalysis outer size is generally consistent with QuikSCAT outer size in the WNP.

CMIP5 experiments

The monthly mean of CIMIP5 from RCP4.5 and RCP8.5 scenarios of July to September is used to derive initial conditions by calculating spatial and temporal averages for a third set of simulations. In this experiment, the CO_2 concentrations are increased for RCP4.5 and RCP8.5 in terms of two stages: current-stage (2011–2040, RCP4.5-C; RCP8.5-C) and future-stage (2071–2100, RCP4.5-F; RCP8.5-F). Based on the above two stages, the initial conditions including T_{atm}, T_{SST}, r_v, surface of r_v, sea level pressure, and geopotential height variations are computed by taking means of the Multi-Model Ensemble (MME) which includes a total of 26 CMIP5 coupled general circulation models (CGCMs) listed in Table 3. The average of different numbers of CMIP5 (see Additional file 1: Table S1) also shows similar patterns (see Additional file 1: Figs. S2 and S3). The N_2O, CH_4, CFC-11, and CFC-12 volume mixing ratios of all the above experiments are set to be the same as CTL at 319, 1774 ppb, 251, and 358 ppt in 2005 values from Intergovernmental Panel on Climate Change (IPCC) (2007) to avoid impacts from other greenhouse gases. The above settings are summarized in Table 1.

Note that all the above experiments are limited by the absence of environmental dynamic forcing such as vertical wind shear. Therefore, the results only reflect thermodynamic mechanisms rather than a realistic atmospheric environment.

Results

Sensitivity experiments

Using the experimental setup described in the previous section, every experiment is run for 144 h. Figure 4a shows the time evolution of TC intensity relative

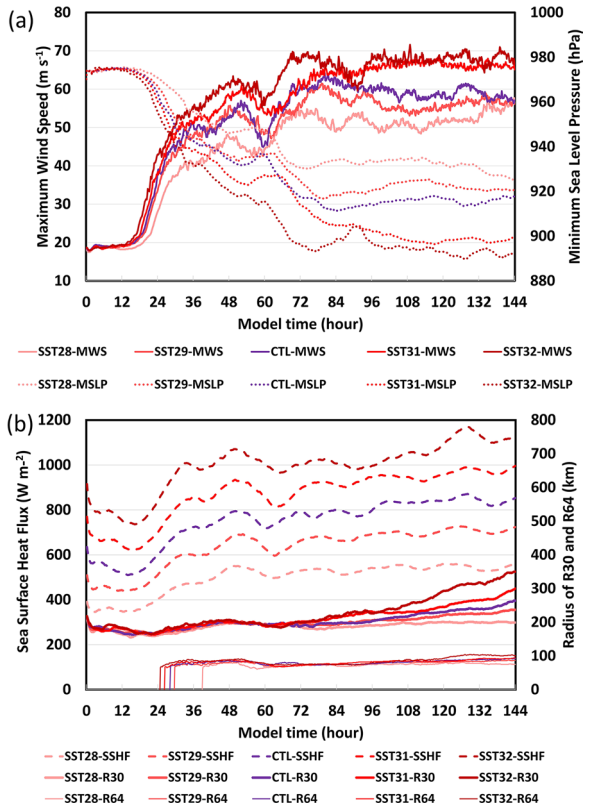

Fig. 4 **a** MSLP (dotted lines) and MWS (solid lines). **b** SSHF (long dashed lines), R30 (thick lines), and R64 (thin lines) of S-SST sensitivity experiments

to minimum sea level pressure (MSLP) and MWS at each 10-min output time in the S-SST experiment. It clearly demonstrates systematic difference in TC intensity for different T_{SST}s during the last 48 h, with greater T_{SST}s corresponding to more intense TCs and increased SSHF (Fig. 4b). The diagnostics of SSHF and r_v are averaged within 300 km of the storm center in the present work (Table 4). As can be seen from there, the initial TC intensity is the same for all experiments while a systematic separation between experiments becomes apparent after 24 h. These results suggest that the increased SSHF may trigger TC intensification, which is consistent with the idea of a positive feedback between TC intensity and SSHF, as described by the theory of WISHE developed in previous studies (Emanuel 1986; Craig and Gray 1996). Based on this widely known result, Fig. 4b shows the time evolution of TC size in terms of R30 and R64. R30 initially remains very similar for all experiments until a systematic separation becomes apparent after about 72 h with greater T_{SST}s leading to a larger R30. The vortex of the S-SST32 experiment is the first to spin up to R64 at around 24 h simulation time. After the vortices in S-SST experiments have spun up to R64, they remain similar at first, but eventually display systematic difference. Larger T_{SST}s produce larger R64, similar to the case of R30. These results show that both the TC size and intensity are positively correlated with SSHF from T_{SST}s in the mature period (96 to 144 h) of our simulations, i.e., larger SSHF from T_{SST}s produce larger, more intense TCs. Note that since the same initial vortex is set for all simulations, the TC intensity and size are related to each other, indicating the discrepancy between the simulations and the real TCs, i.e., the correlation coefficient may not be statistically significant between TC intensity and size in the real atmosphere.

Figure 5 shows the impact of T_{atm} on TC intensity and size. A systematic difference in TC intensity during the last 72 h can be observed (Fig. 5a). Moreover, Fig. 5b shows that the decreased (increased) T_{atm} would lead to increased (decreased) SSHF, which can form a larger (smaller) TC during the mature period with constant underlying T_{SST} in the S-AT experiments. Although the spread of R30 and R64 are smaller than the S-SST experiments, the tendency is quite stable. These simulations are consistent with the results found in Stovern and Ritchie (2016) which indicated that the SSHF is greater in cooler atmosphere. Note that S-AT-2 spins up to R64 earlier than S-AT + 2 without changing the initial r_v in our experiments. Based on the R64 onset time as part of the S-SST and S-AT results, the increasing SSHF causes R64 to occur earlier, which leads to a larger intensification rate in the early TC development stage. Although the result of the R64 onset time may not be robust without an ensemble scheme, it still remains consistent with a previous study (Radu et al. 2014, in their Fig. 4c). This issue will be discussed in the following S-MR of this section.

The positive correlation of T_{SST}s with TC size and intensity as well as the negative correlation of T_{atm} with TC size and intensity described above is clearly important in a global warming scenario where both the atmosphere and oceans are warming. Thus, one is led to the question of which of these two opposing effects will turn out to be stronger. The impact of T_{SST}s on TC intensity described above is consistent with the results of the earlier, more realistic simulation study (Radu et al. 2014) mentioned above, in which a similar positive correlation between T_{SST}s and TC intensity is reported (Shen et al. 2000; Hill and Lackmann 2011; Vecchi et al. 2013; Tuleya 2016). Note that the uniformly increased atmospheric temperature in vertical direction in the idealized simulation would be different from temperature under the atmospheric environment with climate change.

In the S-MR experiments, TC intensity is somewhat increased in the case of S-MR + 10 (Fig. 6). Meanwhile, it appears that on the whole, the impact of r_v on TC size is obviously smaller than that of T_{SST} and T_{atm}, even though

Table 4 Averaged resulting statistics from sensitivity, reanalysis and CMIP5 experiments during 96 to 144 h model time

Experiments	SSHF	r_v	MSLP	MWS	R30	R64
CTL	838.8	16.9	916.0	58.8	230.9	85.4
S-SST28	**545.3 (− 24.3)**	**16.2 (− 2.0)**	**931.7 (7.2)**	**52.0 (− 3.9)**	**197.7 (− 3.0)**	**76.4 (− 3.0)**
S-SST32	**1085.4 (7.0)**	**19.5 (5.2)**	**893.3 (− 15.0)**	**68.0 (7.6)**	**286.3 (3.0)**	**93.6 (1.3)**
S-AT-2	**953.2 (4.0)**	**17.2 (− 0.6)**	**905.3 (− 4.2)**	**62.7 (2.6)**	**280.0 (2.7)**	**90.7 (0.9)**
S-AT + 2	**699.1 (− 8.9)**	**17.7 (2.1)**	**921.8 (2.6)**	**56.4 (− 1.5)**	**213.9 (− 1.6)**	**79.7 (− 1.4)**
S-MR-10	844.7 (0.4)	16.9 (− 0.1)	**918.7 (2.6)**	58.9 (0.1)	233.7 (0.7)	87.8 (0.2)
S-MR + 10	**812.8 (− 1.8)**	17.4 (1.0)	**904.3 (− 7.2)**	**62.8 (2.8)**	226.7 (− 0.3)	82.8 (− 0.8)
S-CO_2 × 2	829.6 (− 0.6)	16.9 (− 0.1)	914.0 (− 0.8)	59.9 (0.8)	227.5 (− 0.2)	82.4 (− 0.9)
S-CO_2 × 4	826.3 (− 0.7)	16.8 (− 0.1)	**909.8 (− 4.8)**	**61.5 (2.3)**	224.0 (− 0.8)	82.2 (− 0.4)
NCEP-M	537.9	17.2	925.7	52.8	191.5	74.1
NCEP-L	531.7 (− 0.5)	**17.4(1.0)**	925.7 (− 0.01)	52.5 (− 0.1)	**187.3 (− 0.7)**	**71.3 (− 1.0)**
CIRES20-P	507.5	16.9	931.7	51.1	189.2	73.6
CIRES20-M	526.4 (1.4)	16.9 (− 0.01)	931.0 (− 0.4)	51.1 (0.02)	189.5 (0.1)	73.3 (− 0.2)
CIRES20-L	**533.6 (1.8)**	**17.1 (1.2)**	932.2 (0.3)	50.4 (− 0.5)	191.5 (0.7)	73.5 (− 0.1)
ERA20C-P	628.2	16.2	926.1	53.1	205.0	78.7
ERA20C-M	632.5 (0.3)	16.3 (0.2)	928.7 (0.6)	52.7 (− 0.1)	210.0 (0.2)	**75.4 (− 1.3)**
ERA20C-L	**608.5 (− 1.2)**	**16.7 (1.4)**	927.0(0.4)	52.6(− 0.2)	**198.9 (− 1.3)**	78.6 (− 0.03)
RCP4.5-C	500.7	17.5	933.3	49.6	190.1	73.5
RCP4.5-F	**522.3 (1.4)**	**18.5 (6.5)**	931.6 (− 0.6)	50.0 (0.2)	190.4 (− 0.1)	72.8 (− 0.3)
RCP8.5-C	507.7 (0.4)	17.5 (0.2)	**929.2 (− 1.6)**	**51.9 (1.3)**	192.6 (0.6)	75.3 (1.1)
RCP8.5-F	***575.6 (5.0;4.3)***	***20.1 (14.8;10.9)***	***922.3 (− 4.5;-5.7)***	***56.3 (3.4;4.7)***	***203.1 (3.5;3.7)***	75.1 (− 0.1;1.1)

The sensitivity experiments are compared to CTL

The NCEP/NCAR R-1 experiments are compared to each other. The CIRES20 and ERA20C experiments are compared to their pre-stage. The future scenarios used in RCP4.5 and RCP8.5 experiments are compared to their current-stage, RCP8.5-C is compared to RCP4.5-C, and RCP8.5-F comparison to RCP8.5-C is shown by italic values. SSHF (*rv*) is the average SSHF (*rv*) within 300 km of the vortex center in units of W m^2 (g kg^{-1}). MSLP (MWS) is minimum sea level pressure (maximum wind speed) in units of hPa (m s^{-1}). R30 and R64 are the azimuthally averaged radius from the vortex center of the 10-m 15 and 32 m s^{-1} wind, respectively. A two-tailed moving-blocks bootstrap-based test with 10,000 resamples and a two-sample *z*-test are used for comparing two means and a null hypothesis of no difference. Bold and italic values indicate significance at the $p < 0.01$ level with an effective degree of freedom around 10. Parenthesized numbers indicate the Cohen's ***d*** effect size of each variable by subtracting the mean of two samples and then dividing the value by the standard deviation. For RCP8.5-F, the first (second) parenthesized number represents the Cohen's ***d*** effect size between RCP8.5-C and RCP8.5-F (RCP4.5-F and RCP8.5-F). There are 289 data samples at 10-min intervals in every experiment ($n = 289$)

the TC intensity diagnostics on S-MR are statistically significant as shown in Table 4. Note that only the r_v in the initial field is adjusted in the S-MR experiments. The result of TC intensity is consistent with findings of Hill and Lackmann (2009). However, the result of TC size is not. They used 20%, 40%, 60% and 80% RH between 100- and 150-km radius for a wide range of RH sensitivity experiments, and also demonstrated that the SSHF could enhance precipitation and generation of the diabatic PV in positive feedback, which further leads to lateral expansion of the TC wind field. In this study, since we focus on the whole TC radius range of r_v experiments, it is difficult to compare the current results to Hill and Lackmann (2009) which showed that the certain environments are associated with a very dry mid- and upper-troposphere (e.g., Saharan air layer; Dunion and Marron 2008). Furthermore, Fig. 6b shows that the first development of R64 is found in S-MR + 10, which is consistent with the finding of Stovern and Ritchie (2016), indicating the rapid development of TC also affected by the environmental specific humidity.

Finally, in the S-CO_2 sensitivity experiments, we consider radiative forcing strengths due to changes in atmospheric CO_2 concentration, without taking into account the adjustment in T_{atm}, T_{SST} or r_v (Fig. 7). Inspection thereof shows that the similar results are obtained in all experiments, with slight differences in TC size, intensity, and SSHF, even though CO_2 concentration is quadrupled, which constitutes an extreme change. Since only radiative forcing is changed in the S-CO_2 experiments, it may be concluded from the results that the impact from the direct radiative forcing is not important for TC development time scales after formation of the storms. It is important to note here that the decreased TC genesis frequency is shown by some of the high-resolution atmospheric global climate models (AGCM) while atmospheric CO_2 concentration is doubled without T_{SST} change (Sugi and Yoshimura 2004; Yoshimura and Sugi 2005; Held and Zhao 2011; Sugi et al. 2012). The upward mass flux

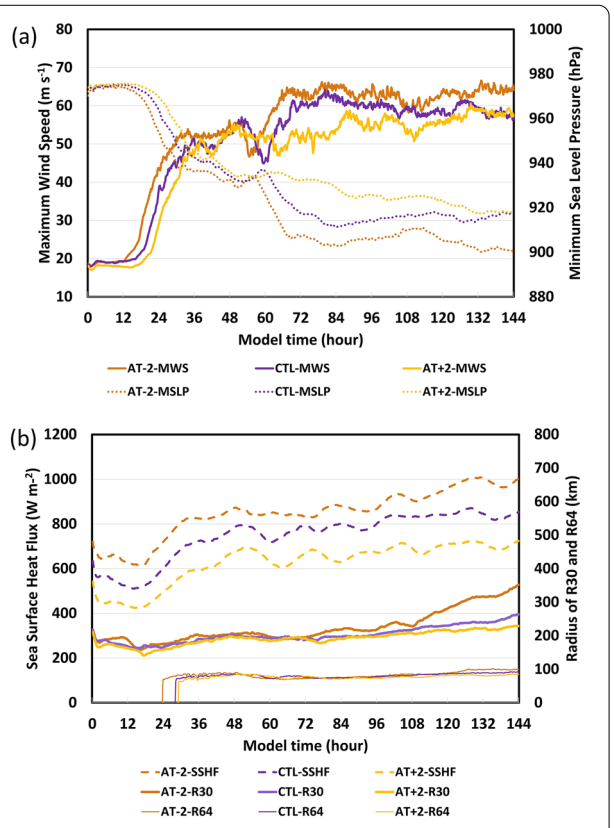

Fig. 5 Same as in Fig. 4, but is for S-AT experiments

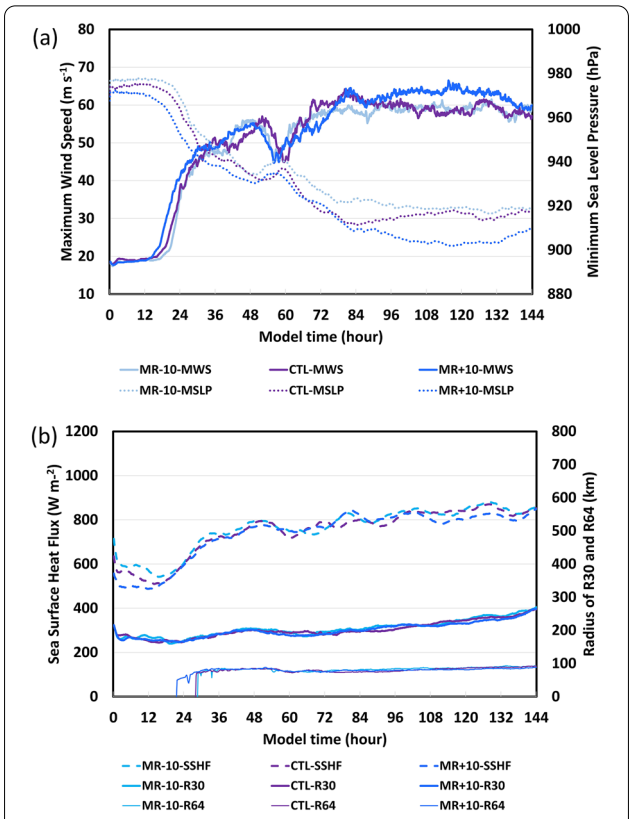

Fig. 6 Same as in Fig. 4, but is for S-MR experiments

hypothesis and saturation deficit hypothesis would require further investigations regarding the possible mechanism of the reduced TC frequency in the future.

Experiments in the past 90 years

The idealized WRF simulations of TCs considering only environmental thermodynamic conditions over the past decades in the WNP are conducted by ERA20C and CIRES20 from 1921 to 2010, and NCEP/NCAR R-1 from 1951 to 2010. Figure 8a shows that the TC intensity in ERA20C experiments is a slightly greater than NCEP and CIRES20 during the late period from 132 to 144 h, because the difference between near-surface T_{atm}s and T_{SST}s of ERA20C is greater than that of NCEP and CIRES20 (Table 1), even though the T_{SST}s among these three reanalysis experiments are quite close, which also corresponds to the SSHF and size (Fig. 8b). Furthermore, there is non-statistically significant difference in average TC intensity of these three reanalysis experiments from 96 to 144 h. However, Table 4 shows a slightly larger R30 of the mid-stage than those of the pre-stage and the later-stage in ERA20C since ERA20C-M also shows a slightly greater difference of near-surface T_{atm} and T_{SST} (Table 1). Meanwhile, the T_{atm}s of ERA20C-L and CIRES20-L increase with altitude under more stable atmosphere, indicating the offsetting effect between the TC outflow and SSHF during TC development (Fig. 2). Vecchi et al. (2013) also mentioned that the increased TC potential intensity is caused by the upper troposphere and the tropical tropopause layer cooling. The initial lower troposphere (about 1000 hPa) temperature of ERA20C-L is about 0.4 K greater than ERA20C-P. In addition, the difference of T_{SST}s between them is about 0.3 K (Table 1), which would also cause SSHF to decrease in Fig. 8b. It is notable that the T_{atm}s of ERA20C-L increase by about 1.2 K in the upper troposphere (about 150 hPa). These probably cause the more stable thermodynamic conditions to hinder TC development, suggesting that the thermodynamic efficiency (ε) of the Carnot cycle (defined by Emanuel 1988) may decrease without considering the dynamic mechanism. Note that there is an earlier time difference of about 6- to 10-h in the onset of R64 CIRES20 compared to the NCEP experiments (Fig. 8c), which is consistent with S-MR since their r_v show a huge difference in Fig. 2a. This provides the necessary link r_v for TC development. Meanwhile, the

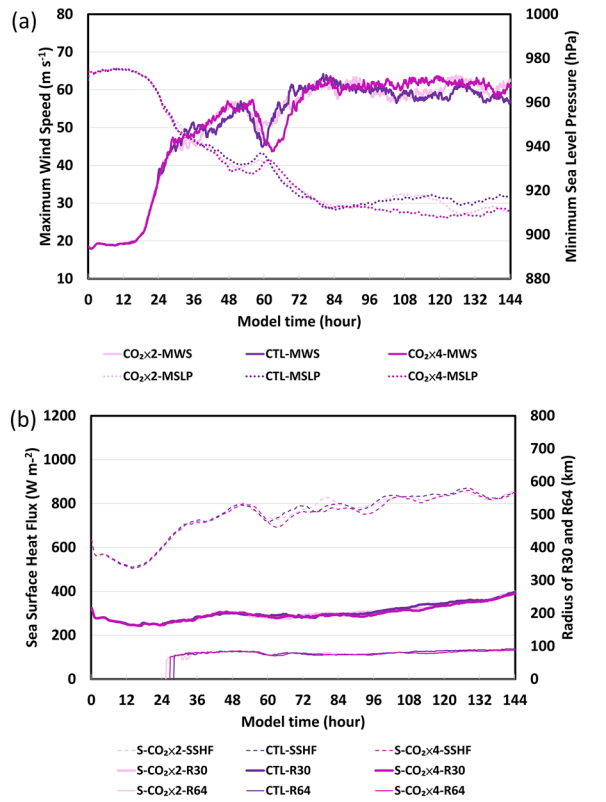

Fig. 7 Same as in Fig. 4, but is for S-CO2 experiments

onset time of R64 between ERA20C and CIRES20 is relatively close, probably due to the impact of increasing T_{atm} that counterweighs the increasing r_v. In these cases, the changed order of environmental thermodynamic conditions may not be great enough to induce significant different development of TCs, although ERA20C-L may capture the tendency of observational TC size (Fig. 3). As a result, the overall Cohen's ***d*** effect sizes show a small difference in reanalysis experiments, even though there are some statistically significant differences in these experiments at the 99% level based on a two-sample z-test with moving-blocks bootstrap.

Experiments under global warming conditions

We perform simulations of TCs under future climate thermodynamic conditions in the WNP in order to investigate the possible change of TC size and intensity and further analyze the physical mechanisms in the idealized WRF model. Using the method described in section "Model and experimental design", we obtain the simulated changes of TC size and intensity for RCP4.5-C, RCP4.5-F, RCP8.5-C, and RCP8.5-F, respectively. We also analyze the time evolution of TC intensity for the experiments initialized using CMIP5 environmental thermodynamic output (Fig. 9a). As a result, the TC in the simulation of the extreme emission scenario (RCP8.5) is about 10% more intense in terms of MWS than that of the intermediate emissions scenario (RCP4.5) in the future climate simulation. Meanwhile, results also show statistically significant increase of TC size (R30) in RCP8.5-F compared to that of RCP8.5-C (10.5 km), which is consistent with Kim et al. (2014) and Yohei et al. (2017). Although there are not huge differences in TC intensity nor size among these experiments in Fig. 9, there is a statistically significant difference in RCP8.5-F as shown in Table 4. As noted earlier, under the influence of significant environmental thermodynamic forcing, it is evident that the TC development is affected by SSHF and r_v during its earlier lifetime. To better understand what mechanism is conductive to the above results in these experiments, the vertical profile of T_{atm} and r_v are investigated in RCP4.5 and RCP8.5. As shown in Fig. 10, T_{atm}s increase acutely from 2011 to 2100, especially in the upper troposphere, near 200 mb. Meanwhile, T_{SST}s also increase by a similar degree as the near-surface T_{atm}s (Table 1). Likewise, the increasing r_v pattern is also found in RCP4.5-F and RCP8.5-F in Fig. 11. Higher r_v is observed near the lower troposphere as time evolves. The r_v of the future-stage in RCP4.5 (RCP8.5) is increased by 5.8% (15.4%) in comparison to the current-stage in RCP4.5 (RCP8.5) at 1000 hPa, and the higher RH is also shown in the middle atmosphere of the RCP4.5 and RCP8.5. This leads to the early onset of R64 during the future scenarios. Note that the TC outflow is at around the 200 hPa level in the idealized WRF model (not shown), which is consistent with Hill and Lackmann (2011). They mentioned that the mitigation effect on TC intensity may be due to the enhancement in the upper-tropospheric warming based on AGCM which exhibits large uncertainty. It can be reasonably speculated that the warming of the upper troposphere and the increase of the outflow height may reduce TC intensity by enhancing the stability instead of by increasing the intensification rate, which is consistent with the findings of Vechhi et al. (2013) and Tuleya et al. (2016). In other words, the relatively stable environment is suppressive for TC development due to the acute increase in T_{atm} in the upper troposphere. Nevertheless, the TC intensity in RCP8.5-F shows an increase when compared to that in the RCP8.5-C, along with the greater Cohen's ***d*** effect sizes (Table 4). This implies that the influence of SSHF could be greater than atmospheric stability.

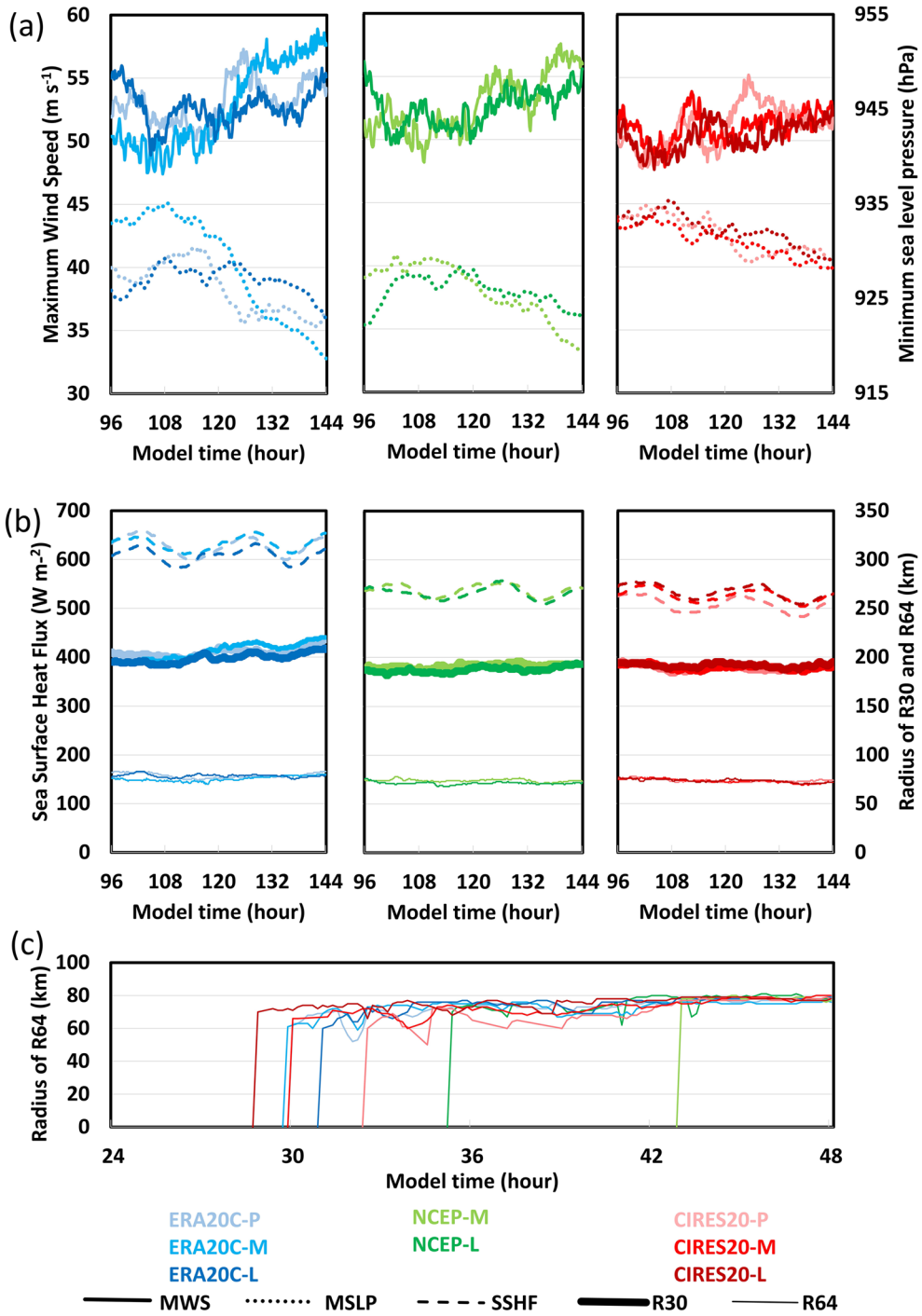

Fig. 8 Same as in Fig. 4, but is distinguished from three reanalysis experiments and for **a** MSLP (dotted lines) and MWS (solid lines); **b** SSHF (long dashed lines), R30 (thick lines), and R64 (thin lines) from 96 to 144 h; **c** R64 in earlier period of reanalysis sensitivity experiments

Discussion

Firstly, it may be noted at this point that the experimental design adopted in this study resembles that of Hill and Lackmann (2011), hereafter HL11. However, there are important differences between their study and the work presented here: (1) they focused on the TC development region in the ALT while we consider the WNP. (2) They used NCEP/NCAR data from 1990 to 1999

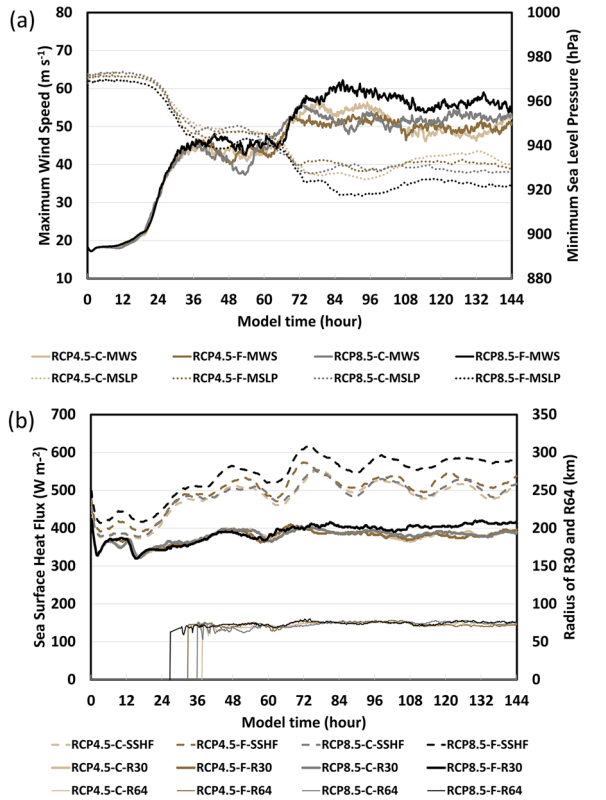

Fig. 9 Same as in Fig. 4, but is for CMIP5 experiments

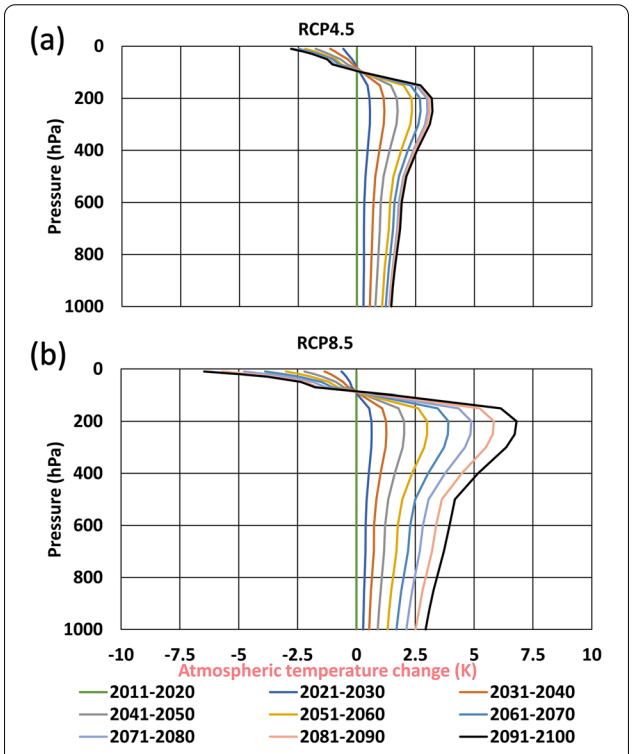

Fig. 10 The difference of averaged T_{atm} in the WNP summer from CMIP5 at **a** RCP4.5, and **b** RCP8.5. The difference is calculated by subtracting the 2011–2020 data from the aggregate data of all

while the NCEP/NCAR reanalysis dataset used in this study covers a far more substantial period, from 1951 to 2010. Moreover, (3) they used data from AR4 (IPCC Fourth Assessment Report) for the future scenario while our analysis is based on more recent CMIP5 data. They found that the TC intensity will increase in the future because of the water vapor and heavier precipitation that induce stronger latent heat release despite a reduction in ε due to warmer outflow temperature, which is seemingly contradictory to the increased TC intensity. Figure 12 shows the T_{atm} tendency in different altitudes from 2021 to 2100, indicating that the decreased ε in outer flow is greater than that of those in the sea surface from RCP8.5 projections. Although a reduction in ε is identified, our results are similar to those of HL11 in that we also find an increase in intensity and size of TC. Figure 10 shows that the upper-tropospheric warming extends more uniformly up to the 150 hPa level in the CMIP5 dataset, which is consistent with Kanada et al. (2020) based on Policy Decision-Making for Future Climate Change (d4PDF) database. According to the maximum potential intensity (MPI) theory, this relatively stronger warming from upper-tropospheric temperature in the CMIP5 dataset may have a suppression effect for the TC development. Notably, Emanuel (1987) indicated that the atmospheric temperature near the sea surface (dT_B) and the mean temperature of the ambient atmosphere at the levels where air flows out of the top of the storm ($d\underline{T}_{out}$) are equal in their simulation, because dT_B and $d\underline{T}_{out}$ are positively correlated in virtually all climate simulations performed at that time, which should be reasonably reflected by the increasing MPI. Emanuel (1991) also indicated that the approximate value of thermodynamic efficiency is 0.3. However, the upper-tropospheric warming of CMIP5 in Fig. 10 and in Fig. 12 should lead to a decreased ε continually. Perhaps the warmer outflow temperature is a secondary factor affecting TC size and intensity as compared to the enhanced SSHF. In this study, the S-AT + 2 resembles RCP8.5-F in T_{SST} (30 °C) and T_{SST} minus near-surface T_{atm} (2 °C), and does not show increased atmospheric stability. Meanwhile, the S-SST28 (30 °C) is also similar to the RCP4.5-C (2 °C) (Table 4). Comparing these two experiments allow a rough evaluation of atmospheric stability (see Additional file 1: Fig. S4). The impact of the increased temperature in the upper-troposphe is partly offset by the increased SSHF when compared with the TC size and intensity of RCP8.5-F (RCP4.5-C) with S-AT + 2 (S-SST28) (see Additional file 1: Fig. S5). Our result is consistent with

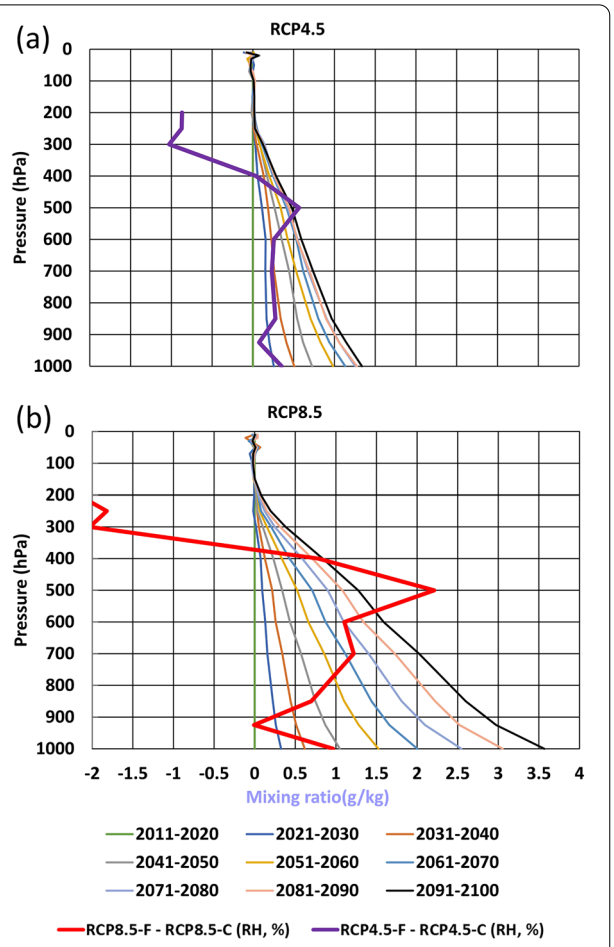

Fig. 11 Same as in Fig. 9, but is for r_v of **a** RCP4.5, and **b** RCP8.5. The purple and red lines are RCP8.5-F minus RCP8.5-C and RCP4.5-F minus RCP4.5-C for relative humidity, respectively

Catto et al. (2011), who also showed a greater warming in the tropical upper troposphere from the simulations of high-resolution global environmental model, even though they focus on the extratropical region. This is probably one of the factors leading to the narrowing of the gap for TC intensity and size between the past and future experiments. Furthermore, Fig. 11 shows that the difference of r_v among these experiments is consistent with the above discussion and HL11, but the r_v effect is negligible in our experiments, while the air–sea thermal disequilibrium continually plays a dominant role in the variation of water vapor. Other studies have found similar discrepancies based on changes in thermodynamic efficiency between simulations and what is suggested by the MPI theory (Shen et al. 2000; Hill and Lackmann 2011; Tuleya et al. 2016).

Secondly, the positive correlation between relative T_{SST}s and TC size identified in our study was also shown in Chavas et al. (2016) by QuikSCAT data. Figure 13 shows the scatter-plots and correlation coefficients of environmental thermodynamic forcing on the SSHF and TC size/intensity. Results show that the correlation between SSHF and TC intensity is greater than that between SSHF and TC size. The correlation coefficient of SSHF and MSLP, SSHF and MWS, SSHF and R30, SSHF and R64 is 0.8543, 0.8416, 0.7714, and 0.7872, respectively. The results also suggest that the correlation coefficient of MWS and R30 is 0.62 (not shown). It is not easy to assess the correlations of MSLP, given that the MSLP is a function of TC size and MWS (Courtney and Knaff 2009; Chavas et al. 2015). Since the initial vortex size is the same in all these idealized simulations, the development period of TC overall may not show the opposite trends between TC intensity and size. However, when the TC enters the dissipation period, the size could expand while intensity decreases, which is consistent with those in the real atmosphere. Therefore, the relationship between the intensity and size of TC is yet to be validated by high-resolution observations in the future.

Thirdly, the direct effects of radiative forcing due to CO_2 concentration are negligible, shedding some new light on previous works where $2\times CO_2$ or $4\times CO_2$ was found to increase TC intensity (Knutson et al. 2010; Bell et al. 2013; Emanuel 2013; Villarini and Vecchi 2013; Wang and Wu 2015). Undoubtedly, a substantial increase in CO_2 concentration could cause overall changes on a global scale, including increasing T_{SST}, T_{atm} and r_v. These changes then affect TC intensity as found in previous studies. However, we have investigated domain-average outgoing longwave radiation (OLR) at the top of the clear sky from our CO_2 sensitivity experiments and found that the OLR of S-$CO_2\times 4$ is smaller than CTL by about 30 W m^{-2} in the earlier model time, and eventually becomes similar (not shown). In addition, the CO_2 concentration in year 2159 is shown to be 1519 ppm (close to S-$CO_2\times 4$) for RCP8.5, indicating radiative forcing of about 11 W m^{-2} in Fig. 6 of Meinshausen et al. (2011). Since the dominant gaseous absorber of infrared radiation is water vapor, the radiative forcing of CO_2 is relatively unapparent in the TC life cycle. The viewpoint of this study confirms Sugi and Yoshimura (2004) who distinguished between the impacts from T_{SST}s and that from CO_2 concentration.

Conclusions

In this study, the past, current and future variations of TC size and intensity have been investigated using the idealized WRF model over the WNP. The results of sensitivity experiments with varying thermodynamic conditions presented here indicate a major role of SSHF, the air–sea thermal disequilibrium, and the atmospheric temperature in determining the TC size and intensity. In

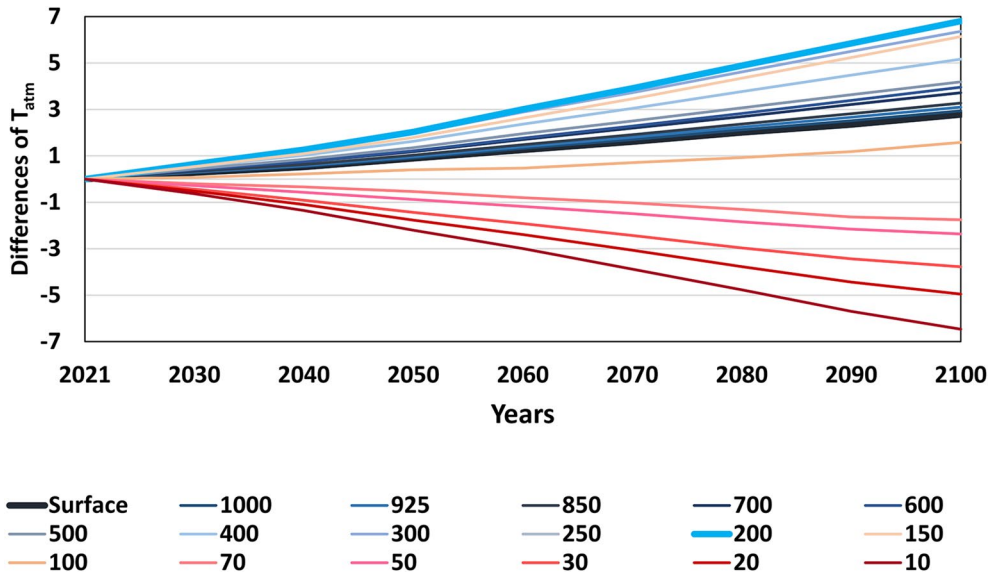

Fig. 12 The tendency for differences of T_{atm} in different altitudes from 2021 to 2100. Blue line is 200 hPa level, and black line represents T_{SST}

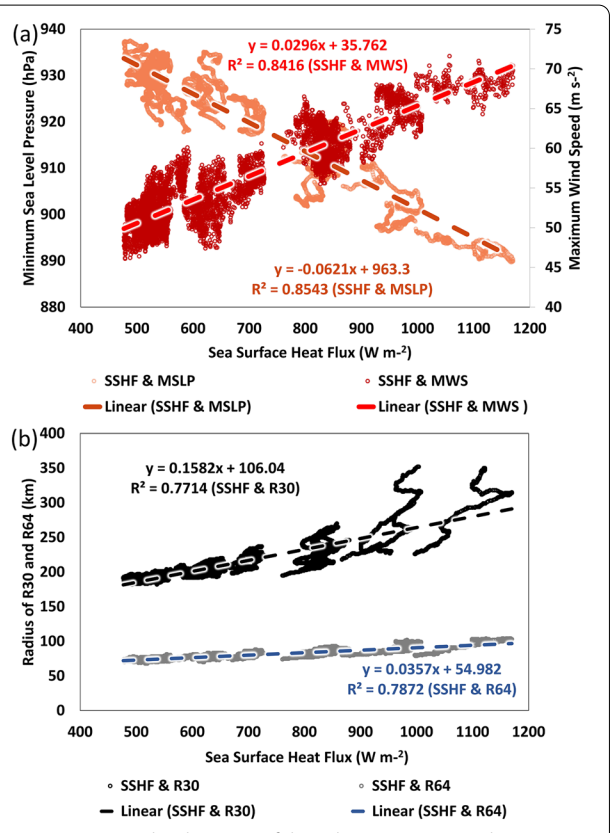

Fig. 13 Scatter-plot diagrams of the subsequent 96–144 h SSHF against **a** MSLP and MWS, **b** R30 and R64. The dashed lines are the best-fit lines. The R^2 from the regression equation and percentage variance is also listed among the TC intensity and size parameters

general, T_{SST} increases would be accompanied by SSHF increases; increased T_{atm} would reduce the SSHF in model experiments and vice versa. This result is consistent with the findings of Radu et al. (2014) in which cases were simulated using a more realistic model. In contrast to their study, our results avoid uncertainties arising from track effects and vertical wind shear since environmental dynamic forcing is set to zero and experiments are performed on an f-plane.

The results of the experiments under the past climate thermodynamic conditions presented here suggest that the overall climatological TC size and intensity in the WNP have similar patterns in the past 90 years. Although the later stages of the ERA20C show a slightly smaller TC size as compared to past simulations, the Cohen's ***d*** effect size is relatively small (Table 4). On the other hand, Wu et al. (2005) found an increasing trend in TC intensity in the WNP between 1965 and 2003 (see also Webster et al. 2005; Kamahori et al. 2006; Elsner et al. 2008; Kossin et al. 2013, 2016). These results are not uncontroversial as pointed out in Wu and Zhao (2012), since improvement in observational capabilities for TC intensity occurred in 1965, while availability of TC size data does not date back quite as far.

We also find that the climatological TC size and intensity in the WNP (based on CMIP5 data) will both increase slightly under the future warming climate according to our simulations, associated with a significant warming of the whole troposphere and T_{SST} in the CMIP5 data compared with the current-stage climate of the averaged environment between 2011 and 2040

(Fig. 10; Table 1). The present study provides a reference of using the idealized WRF model for investigating changes of TC size and intensity under the environmental thermodynamic conditions of future global warming. To our best knowledge, our sensitivity investigation of TC size further explains the mechanism of CMIP5 response under future (global warming) environmental thermodynamic conditions based on idealized WRF regional numerical simulations. The global CGCM study of Kim et al. (2014) and the downscaled study by Knutson et al. (2015) using the GFDL Hurricane Model reach conflicting conclusions on the TC size changes in the WNP. Kim et al. (2014) reported a slightly increased TC size for the global mean and WNP, while Knutson et al. (2015) found a decreased relative frequency of median values in TC size in the WNP that offsets increase in other basins. Our results support the findings of Kim et al. (2014), in the sense that both are similar to the prediction of MPI by Emanuel (1995), as pointed out in Lin and Emanuel (2016), namely that the TC size should increase under environmental thermodynamic conditions of future global warming. Our projection of a future increase in TC intensity is also similar to some earlier studies such as that by Bell et al. (2013) who reported a slight increase in TC intensity in the WNP from a CGCM run under future $4 \times CO_2$ conditions. Knutson et al. (2010) similarly suggested that the global averaged intensity of TCs will increase in the future due to global warming. However, in their Fig. 1, while there is an increase in the mean TC intensity, the high-resolution dynamical models can vary over a range of around $\pm 15\%$ or more. Further study is needed to analyze the difference in TC size and intensity.

A comparison between the past climate and future climate based on our experiments suggests that when the impact of the increase in T_{SST} is smaller than that in T_{atm} such as in the reanalysis experiments, the TC will be suppressed. However, these RCP experiments also show different features of TC size and intensity via the thermodynamic nonlinear process by combining the effects of SSHF, T_{SST}, r_v, CO_2, and T_{atm} in the upper and lower troposphere. Future work will also be necessary for more detailed investigations of certain results presented here. Firstly, further experiments are required to distinguish the effect of SSHF and atmospheric stability. Secondly, our experimental design rules out the possibility that the simulated changes in TC size and intensity in the future climate experiment are a result of the environmental wind field, focusing on the air–sea thermal disequilibrium and the stable atmospheric conditions. However, since TCs in the real atmosphere are subject to environmental dynamic forcing, the impact of such forcing remains to be determined. Therefore, future work with regional models using the downscaling technique and including environmental dynamic forcing is necessary to verify the accuracy of our findings. Thirdly, the high correlation between size and intensity in our experiments calls for further investigations to clarify which factors are responsible for the observed low correlation between size and intensity of real TCs. Finally, to ensure robust results, the ensemble simulations are also needed as in previous studies (Kanada et al. 2020).

Supplementary Information

The online version contains supplementary material available at https://doi.org/10.1186/s40562-022-00239-6.

Additional file 1. Additional figures and table.

Acknowledgements

This work is supported by the Ministry of Science and Technology of Taiwan under Grants MOST 109-2123-M-002-003- and MOST 110-2123-M-002-010-, and by the Office of Naval Research through Grant N00014-20-1-2467.

Author contributions

Chun-Chieh Wu and Kun-Hsuan Chou provided supervision, financial support, and comments for this study, and checked/corrected all the versions of the manuscript. Cheng-Hsiang Chih collected research data, conducted data analyses, and prepared the manuscript. All authors read and approved the final manuscript.

Funding

This work is funded by the Ministry of Science and Technology of Taiwan under Grants MOST 109-2123-M-002-003- and MOST 110-2123-M-002-010-, and by the Office of Naval Research through Grant N00014-20-1-2467.

Availability of data and materials

ECMWF for providing the ERA-20C data (https://www.ecmwf.int/en/forecasts/datasets/reanalysis-datasets/era-20c). NCEP and NCAR for providing the R-1 reanalysis data (https://rda.ucar.edu/datasets/ds090.0/). We thank and NOAA for providing the CIRES 20th Reanalysis V2 data (https://psl.noaa.gov/data/gridded/data.20thC_ReanV2.pressure.html). CMIP5 data were download online (https://esgf-node.llnl.gov/search/cmip5/), as were QuickSCAT data (https://www.remss.com/missions/qscat/). Model datasets and materials analyzed in this study are accessible from the corresponding author under reasonable request.

Declarations

Competing interests

The authors declare that they have no competing interests.

Author details

[1]Department of Atmospheric Sciences, National Taiwan University, No. 1, Sec. 4, Roosevelt Rd, Taipei 10617, Taiwan. [2]Department of Atmospheric Sciences, Chinese Culture University, Taipei, Taiwan. [3]Research Center for Environmental Changes, Academia Sinica, Taipei, Taiwan.

Received: 29 October 2021 Accepted: 25 July 2022
Published online: 05 September 2022

References

Bel R, Strachan J, Vidale PL, Hodges K, Roberts M (2013) Response of tropical cyclones to idealized climate change experiments in a global

high-resolution coupled general circulation model. J Clim 26:7966–7980. https://doi.org/10.1175/JCLI-D-12-00749.1
Bolton D (1980) The computation of equivalent potential temperature. Mon Wea Rev 108:1046–1053. https://doi.org/10.1175/1520-0493(1980)108%3c1046:TCOEPT%3e2.0.CO;2
Catto JL, Shaffrey LC, Hodges KI (2011) Northern Hemisphere extratropical cyclones in a warming climate in the HiGEM high-resolution climate model. J Clim 24:5336–5352. https://doi.org/10.1175/2011JCLI4181.1
Chan JCL (1985) Tropical cyclone activity in the northwest Pacific in relation to the El Ni n o/Southern Oscillation phenomenon. Mon Wea Rev 113:599–606. https://doi.org/10.1175/1520-0493(1985)113%3c0599:TCAITN%3e2.0.CO;2
Chan JCL (2000) Tropical cyclone activity over the western North Pacific associated with El Ni n o and La Ni n a events. J Clim 13:2960–2972. https://doi.org/10.1175/1520-0493(1985)113%3c0599:tcaitn%3e2.0.co;2
Chan KTF, Chan JCL (2012) Size and strength of tropical cyclones as inferred from QuikSCAT data. Mon Wea Rev 140:811–824. https://doi.org/10.1175/MWR-D-10-05062.1
Chan KTF, Chan JCL (2014) Impacts of initial vortex size and planetary vorticity on tropical cyclone size. Q J R Meteorol Soc 140:2235–2248. https://doi.org/10.1002/qj.2292
Chan JCL, Liu K-S (2004) Global warming and western North Pacific typhoon activity from an observational perspective. J Clim 17:4590–4602. https://doi.org/10.1175/3240.1
Chavas DR, Emanuel KA (2010) A QuikSCAT climatology of tropical cyclone size. Geophys Res Lett 37:L18816. https://doi.org/10.1029/2010GL044558
Chavas DR, Emanuel KA (2014) Equilibrium tropical cyclone size in an idealized state of axisymmetric radiative–convective equilibrium. J Atmos Sci 71(5):1663–1680. https://doi.org/10.1175/JAS-D-13-0155.1
Chavas DR, Lin N, Emanuel KA (2015) A Model for the complete radial structure of the tropical cyclone wind field. Part I: comparison with observed structure. J Atmos Sci 72:3647–3662. https://doi.org/10.1175/JAS-D-15-0014.1
Chavas DR, Lin N, Dong W, Lin Y (2016) Observed tropical cyclone size revisited. J Clim 29:2923–2939. https://doi.org/10.1175/JCLI-D-15-0731.1
Chen W-Y (1982) Fluctuation in Northern Hemisphere 700 mb height field associated with the Southern Oscillation. Mon Wea Rev 110:808–823. https://doi.org/10.1175/1520-0493(1982)110%3c0808:FINHMH%3e2.0.CO;2
Chia H-H, Ropelewski CF (2002) The interannual variability in the genesis location of tropical cyclones in the northwest Pacific. J Clim 15:2934–2944. https://doi.org/10.1175/1520-0442(2002)015%3c2934:TIVITG%3e2.0.CO;2
Chih C-H, Chou K-H, Chiao S (2015) Topography and tropical cyclone structure influence on eyewall evolution in Typhoon Sinlaku (2008). Terr Atmos Ocean Sci 26:571–586. https://doi.org/10.3319/TAO.2015.05.08.01(A)
Cocks SB, Gray WM (2002) Variability of the outer wind profiles of western North Pacific typhoons: Classifications and techniques for analysis and forecasting. Mon Wea Rev 130:1989–2005. https://doi.org/10.1175/1520-0493(2002)130%3c1989:VOTOWP%3e2.0.CO;2
Cohen J (1988) Statistical Power Analysis for the Behavioral Sciences (2nd ed.), Routledge, ISBN 978–0–8058–0283–2. doi:https://doi.org/10.4324/9780203771587.
Compo GP et al (2011) The Twentieth Century Reanalysis Project. Quarterly J Roy Meteorol Soc 137:1–28. https://doi.org/10.1002/qj.776
Courtney J, Knaff JA (2009) Adapting the Knaff and Zehr wind–pressure relationship for operational use in Tropical Cyclone Warning Centres. Aust Meteorol Oceanogr J 58:167–179. https://doi.org/10.22499/2.5803.002
Craig GC, Gray SL (1996) CISK or WISHE as the mechanism for tropical cyclone intensification. J Atmos Sci 53:3528–3540. https://doi.org/10.1175/1520-0469(1996)053%3c3528:COWATM%3e2.0.CO;2
Davis RE (1976) Predictability of sea-surface temperature and sea-level pressure anomalies over the North Pacific Ocean. J Phys Oceanogr 6:249–266. https://doi.org/10.1175/1520-0485(1976)006%3c0249:POSSTA%3e2.0.CO;2
Dean L, Emanuel KA, Chavas DR (2009) On the size distribution of Atlantic tropical cyclones. Geophys Res Lett 36:L14803. https://doi.org/10.1029/2009GL039051
DeMaria M, Pickle JD (1988) A simplified system of equations for simulation of tropical cyclones. J Atmos Sci 45:1542–1554. https://doi.org/10.1175/1520-0469(1988)045%3c1542:ASSOEF%3e2.0.CO;2
Dunion JP, Marron CS (2008) A reexamination of the Jordan mean tropical sounding based on awareness of the Saharan air layer: results from 2002. J Clim 21:5242–5253. https://doi.org/10.1175/2008JCLI1868.1
Elsner JB, Kossin JP, Jagger TH (2008) The increasing intensity of the strongest tropical cyclones. Nature 455:92–95. https://doi.org/10.1038/nature07234
Emanuel KA (1986) An air-sea interaction theory for tropical cyclones. Part I: Steady-state maintenance. J Atmos Sci 43:585–605. https://doi.org/10.1175/1520-0469(1986)043%3c0585:AASITF%3e2.0.CO;2
Emanuel KA (1987) The dependence of hurricane intensity on climate. Nature 326:483–485. https://doi.org/10.1038/326483a0
Emanuel KA (1988) The Maximum Intensity of Hurricanes. J Atmos Sci 45:1143–1155. https://doi.org/10.1175/1520-0469(1988)045%3c1143:TMIOH%3e2.0.CO;2
Emanuel KA (1991) The theory of hurricanes. Annu Rev Fluid Mech 23:179–196. https://doi.org/10.1146/annurev.fl.23.010191.001143
Emanuel KA (1995) Sensitivity of tropical cyclones to surface exchange coefficients and a revised steady-state model incorporating eye dynamics. J Atmos Sci 52:3969–3976. https://doi.org/10.1175/1520-0469(1995)052%3c3969:SOTCTS%3e2.0.CO;2
Emanuel KA (2005) Increasing destructiveness of tropical cyclones over the past 30 years. Nature 436:686–688. https://doi.org/10.1038/nature03906
Emanuel KA (2013) Downscaling CMIP5 climate models shows increased tropical cyclone activity over the 21st century. Proc Natl Acad Sci USA 110:12219–12224. https://doi.org/10.1073/pnas.1301293110
Emanuel KA, Wing AA, Vincent EM (2014) Radiative-convective instability. J Adv Model Earth Syst 6:75–90. https://doi.org/10.1002/2013MS000270
Grinsted A, Moore JC, Jevrejeva S (2012) Homogeneous record of Atlantic hurricane surge threat since 1923. Proc Natl Acad Sci USA 109(48):19601–19605. https://doi.org/10.1073/pnas.1209542109
Gutmann ED et al (2018) Changes in hurricanes from a 13-year convection-permitting pseudo global warming simulation. J Clim 31:3643–3657. https://doi.org/10.1175/JCLI-D-17-0391.1
Hakim GJ (2011) The mean state of axisymmetric hurricanes in statistical equilibrium. J Atmos Sci 68:1364–1376. https://doi.org/10.1175/2010JAS3644.1
Harris DL (1963) Characteristics of the Hurricane Storm Surge, Technical Paper No. 48 (US Department of Commerce, Weather Bureau, Washington, DC). Available at www. csc.noaa.gov/hes/images/pdf/CHARACTERISTICS_STORM_SURGE.pdf.
Hasegawa A, Emori S (2007) Effect of air-sea coupling in the assessment of CO2-induced intensification of tropical cyclone activity. Geophys Res Lett 34:L05701. https://doi.org/10.1029/2006GL028275
He F, Posselt DJ, Zarzycki CM, Jablonowski C (2015) A balanced tropical cyclone test case for AGCMs with background vertical wind shear. Mon Wea Rev 143:1762–1781. https://doi.org/10.1175/MWR-D-14-00366.1
Held IM, Zhao M (2011) The response of tropical cyclone statistics to an increase in CO_2 with fixed sea surface temperatures. J Clim 24:5353–5364. https://doi.org/10.1175/JCLI-D-11-00050.1
Hill KA, Lackmann GM (2009) Influence of environmental humidity on tropical cyclone size. Mon Wea Rev 137:3294–3315. https://doi.org/10.1175/2009MWR2679.1
Hill KA, Lackmann GM (2011) The impact of future climate change on TC intensity and structure: a downscaling approach. J Clim 24:4644–4661. https://doi.org/10.1175/2011JCLI3761.1
Ho C-H, Baik J-J, Kim J-H, Gong D-Y, Sui CH (2004) Interdecadal changes in summertime typhoon tracks. J Clim 17:1767–1776. https://doi.org/10.1175/1520-0442(2004)017%3c1767:ICISTT%3e2.0.CO;2
Ho C-H, Kim J-H, Jeong J-H, Kim H-S, Chen D (2006) Variation of tropical cyclone activity in the south Indian Ocean: El Ni n o-Southern Oscillation and Madden-Julian Oscillation effects. J Geophys Res 111:D22101. https://doi.org/10.1029/2006JD007289
Hong S-Y, Noh Y, Dudhia J (2006) A new vertical diffusion package with an explicit treatment of entrainment processes. Mon Wea Rev 134:2318–2341. https://doi.org/10.1175/MWR3199.1

Huang C-Y, Wong C-S, Yeh T-C (2011) Extreme rainfall mechanisms exhibited by Typhoon Morakot (2009). Terr Atmos Oceanic Sci 22:613–632. https://doi.org/10.3319/TAO.2011.07.01.01(TM)
Iacono MJ, Delamere JS, Mlawer EJ, Shephard MW, Clough SA, Collins WD (2008) Radiative forcing by long-lived greenhouse gases: Calculations with the AER radiative transfer models. J Geophys Res 113:D13103. https://doi.org/10.1029/2008JD009944
Irish JL, Resio DT, Ratcliffe JJ (2008) The influence of storm size on hurricane surge. J Phys Oceanogr 38:2003–2013. https://doi.org/10.1175/2008JPO3727.1
Jimenez PA, Dudhia J, Gonzalez-Rouco JF, Navarro J, Montavez JP, Garcia-Bustamante E (2012) A revised scheme for the WRF surface layer formulation. Mon Wea Rev 140:898–918. https://doi.org/10.1175/MWR-D-11-00056.1
Jordan CL (1958) Mean soundings for the West Indies area. J Meteor 15:91–97. https://doi.org/10.1175/1520-0469(1958)015%3c0091:MSFTWI%3e2.0.CO;2
Kalnay E et al (1996) The NCEP/NCAR 40-Year Reanalysis Project. Bull Amer Meteor Soc 77:437–471. https://doi.org/10.1175/1520-0477(1996)077,0437:TNYRP.2.0.CO;2
Kamahori HN, Yamazaki N, Mannoji N, Takahashi K (2006) Variability in intense tropical cyclone days in the western North Pacific. SOLA 2:104–107. https://doi.org/10.2151/sola.2006-027
Kanada S, Tsuboki K, Takayabu I (2020) Future changes of tropical cyclones in the midlatitudes in 4-km-mesh downscaling experiments from large-ensemble simulations. SOLA 16:57–63. https://doi.org/10.2151/sola.2020-010
Khairoutdinov M, Emanuel KA (2013) Rotating radiative-convective equilibrium simulated by a cloud-resolving model. JAMES 5:816–825. https://doi.org/10.1002/2013MS000253
Kim H-S, Vecchi GA, Knutson TR, Anderson WG, Delworth TL, Rosati A, Zeng F, Zhao M (2014) Tropical cyclone simulation and response to CO2 doubling in the GFDL CM2.5 high-resolution coupled climate model. J Clim 27:8034–8054. https://doi.org/10.1175/JCLI-D-13-00475.1
Kimball SK, Mulekar MS (2004) A 15-year climatology of North Atlantic tropical cyclones Part I: size parameters. J Clim 17:3555–3575. https://doi.org/10.1175/1520-0442(2004)017%3c3555:AYCONA%3e2.0.CO;2
Klotzbach PJ (2006) Trends in global tropical cyclone activity over the past twenty years (1986–2005). Geophys Res Lett 33:L10805. https://doi.org/10.1029/2006GL025881
Knaff AJ, Longmore SP, Molenar DA (2014) An objective satellite-based tropical cyclone size climatology. J Clim 27:455–476. https://doi.org/10.1175/JCLI-D-13-00096.1
Knutson TR, Coauthors, (2020) Tropical cyclones and climate change assessment part II: projected response to anthropogenic warming. Bull Amer Meteor Soc 101:E303–E322. https://doi.org/10.1175/BAMS-D-18-0194.1
Knutson TR, McBride JL, Chan J, Emanuel KA, Holland G, Landsea C, Held I, Kossin JP, Srivastava AK, Sugi M (2010) Tropical cyclones and climate change. Nat Geosci 3:157–163. https://doi.org/10.1038/ngeo779
Knutson TR, Sirutis JJ, Zhao M, Tuleya RE, Bender MA, Vecchi GA, Villarini G, Chavas D (2015) Global projections of intense tropical cyclone activity for the late twenty-first century from dynamical downscaling of CMIP5/RCP4.5 scenarios. J Clim 28:7203–7224. https://doi.org/10.1175/JCLI-D-15-0129.1
Knutson TR, Camargo SJ, Chan JCL, Emanuel KA, Ho CH, Kossin JP, Mohapatra M, Satoh M, Sugi M, Walsh K, Wu L (2019) Tropical cyclones and climate change assessment: Part I. Detection and attribution. Bull Amer Meteor Soc 100:1987–2007. https://doi.org/10.1175/BAMS-D-18-0189.1
Kossin JP, Olander TL, Knapp KR (2013) Trend analysis with a new global record of tropical cyclone intensity. J Clim 26:9960–9976. https://doi.org/10.1175/JCLI-D-13-00262.1
Kossin JP, Emanuel KA, Camargo SJ (2016) Past and projected changes in Western North Pacific tropical cyclone exposure. J Clim 29:5725–5739. https://doi.org/10.1175/JCLI-D-16-0076.1
Kun-Hsuan, Chou Chun-Chieh, Wu Yuqing, Wang (2011) Eyewall Evolution of Typhoons Crossing the Philippines and Taiwan: An Observational Study. Terr Atmos Oceanic Sci 22(6):535. https://doi.org/10.3319/TAO.2011.05.10.01(TM)
Lander MA (1994) Description of a monsoon gyre and its effects on the tropical cyclones in the western North Pacific during August 1991. Wea Forecast 9:640–654. https://doi.org/10.1175/1520-0434(1994)009%3c0640:DOAMGA%3e2.0.CO;2
Lee C-S, Cheung KK-W, Fang W-T, Elsberry RL (2010) Initial maintenance of tropical cyclone size in the western North Pacific. Mon Wea Rev 138:3207–3223. https://doi.org/10.1175/2010MWR3023.1
Li T, Ge X, Peng M, Wang W (2012) Dependence of tropical cyclone intensification on the Coriolis parameter. Trop Cyclone Res Rev 1:242–253. https://doi.org/10.6057/2012TCRR02.04
Lin N, Emanuel KA (2016) Grey swan tropical cyclones. Nat Clim Chang 6:106–111. https://doi.org/10.1038/nclimate2777
Liu K-S, Chan JCL (1999) Size of tropical cyclones as inferred from ERS-1 and ERS-2 data. Mon Wea Rev 127:2992–3001. https://doi.org/10.1175/1520-0493(1999)127%3c2992:SOTCAI%3e2.0.CO;2
Liu K-S, Chan JCL (2002) Synoptic flow patterns associated with small and large tropical cyclones over the western North Pacific. Mon Wea Rev 130:2134–2142. https://doi.org/10.1175/1520-0493(2002)130%3c2134:SFPAWS%3e2.0.CO;2
Liu W-T, Katsaros KB, Businger JA (1979) Bulk parameterization of air-sea exchanges of heat and water vapor including the molecular constraints at the interface. J Atmos Sci 36:1722–1735. https://doi.org/10.1175/1520-0469(1979)036%3c1722:BPOASE%3e2.0.CO;2
Matsuura T, Yumoto M, Iizuka S (2003) A mechanism of interdecadal variability of tropical cyclone activity over the western North Pacific. Clim Dyn 21:105–117. https://doi.org/10.1007/s00382-003-0327-3
Meehl G, Covey C, Delworth T, Latif M, McAvaney B, Mitchell J, Stouffer R, Taylor K (2007) The WCRP CMIP3 multimodel dataset: a new era in climate change research. Bull Amer Meteor Soc 88:1383–1394. https://doi.org/10.1175/BAMS-88-9-1383
Meinshausen M et al (2011) The RCP Greenhouse Gas Concentrations and their extension from 1765 to 2300. Clim Change 109:213–214. https://doi.org/10.1007/s10584-011-0156-z
Merrill RT (1984) A comparison of large and small tropical cyclones. Mon Wea Rev 112:1408–1418. https://doi.org/10.1175/1520-0493(1984)112%3c1408:ACOLAS%3e2.0.CO;2
Nguyen HV, Chen Y-L (2011) High-resolution initialization and simulations of Typhoon Morakot (2009). Mon Wea Rev 139:1463–1491. https://doi.org/10.1175/2011MWR3505.1
Nolan DS, Rappin ED, Emanuel KA (2007) Tropical cyclogenesis sensitivity to environmental parameters in radiative–convective equilibrium. Q J R Meteorol Soc 133:2085–2107. https://doi.org/10.1002/qj.170
Oouchi K, Yoshimura J, Yoshimura H, Mizuta R, Kusunoki S, Noda A (2006) Tropical cyclone climatology in a global-warming climate as simulated in a 20 km-mesh global atmospheric model: frequency and wind intensity analyses. J Meteor Soc Japan 84:259–276. https://doi.org/10.2151/jmsj.84.259
Parker WS (2016) Reanalyses and observations: What's the difference? Bull Amer Meteor Soc 97:1565–1572. https://doi.org/10.1175/BAMS-D-14-00226.1
Poli P et al (2016) ERA-20C: an atmospheric reanalysis of the twentieth century. J Clim 29:4083–4097. https://doi.org/10.1175/JCLI-D-15-0556.1
Radu R, Toumi R, Phau J (2014) Influence of atmospheric and sea surface temperature on the size of hurricane Catarina. Q. J. R.Meteorol. Soc 140:1778–1784. https://doi.org/10.1002/qj.2232
Rotunno R, Emanuel KA (1987) An air-sea interaction theory for tropical cyclones. Part II: Evolutionary study using a nonhydrostatic axisymmetric numerical model. J Atmos Sci 44:542–561. https://doi.org/10.1175/1520-0469(1987)044%3c0542:AAITFT%3e2.0.CO;2
Shen W, Tuleya RE, Ginis I (2000) A sensitivity study of thermodynamic environment on GFDL model hurricane intensity: Implications for global warming. J Clim 13:109–121. https://doi.org/10.1175/1520-0442(2000)013%3c0109:ASSOTT%3e2.0.CO;2
Skamarock WC et al. (2008) A description of the Advanced Research WRF version 3. NCAR Tech. Note NCAR/TN-4751STR, 113 pp. https://doi.org/10.5065/D68S4MVH.
Stovern DR, Ritchie EA (2016) Simulated sensitivity of tropical cyclone size and structure to the atmospheric temperature profile. J Atmos Sci 73:4553–4571. https://doi.org/10.1175/JAS-D-15-0186.1
Sugi M, Yoshimura J (2004) A mechanism of tropical precipitation change due to CO2 increase. J Clim 17:238–243. https://doi.org/10.1175/1520-0442(2004)017%3c0238:AMOTPC%3e2.0.CO;2

Sugi M, Murakami H, Yoshimura J (2012) On the mechanism of tropical cyclone frequency changes due to global warming. J Meteor Soc Japan 90A:397–408. https://doi.org/10.2151/jmsj.2012-A24
Taylor KE, Stouffer RJ, Meehl GA (2012) An overview of CMIP5 and the experiment design. Bull Amer Meteorol Soc 93:485–498. https://doi.org/10.1175/BAMS-D-11-00094.1
Thompson G, Field PR, Rasmussen RM, Hall WD (2008) Explicit forecasts of winter precipitation using an improved bulk microphysics scheme. Part II: Implementation of a new snow parameterization. Mon Wea Rev 136:5095–5115. https://doi.org/10.1175/2008MWR2387.1
Thorne PW, Vose RS (2010) Reanalyses suitable for characterizing long-term trends. Bull Amer Meteor Soc 91:353–361. https://doi.org/10.1175/2009BAMS2858.1
Tu J-Y, Chou C, Chu P-S (2009) The abrupt shift of typhoon activity in the vicinity of Taiwan and its association with western North Pacific-East Asian climate change. J Clim 22:3617–3628. https://doi.org/10.1175/2009JCLI2411.1
Tuleya RE, Bender M, Knutson TR, Sirutis JJ, Thomas B, Ginis I (2016) Impact of upper-tropospheric temperature anomalies and vertical wind shear on tropical cyclone evolution using an idealized version of the operational GFDL hurricane model. J Atmos Sci 73:3803–3820. https://doi.org/10.1175/JAS-D-16-0045.1
Vecchi GA et al. Impacts of atmospheric temperature trends on tropical cyclone activity. J Clim 2013. https://doi.org/10.1175/JCLI-D-12-00503.1.
Villarini G, Vecchi GA (2013) Projected increases in North Atlantic tropical cyclone intensity from CMIP5 models. J Clim 26:3231–3240. https://doi.org/10.1175/JCLI-D-12-00441.1
Wang B, Chan JCL (2002) How strong ENSO events affect tropical storm activity over the Western North Pacific. J Clim 15:1643–1658. https://doi.org/10.1175/1520-0442(2002)015%3c1643:HSEEAT%3e2.0.CO;2
Wang C, Wu LG (2015) Influence of future tropical cyclone track changes on their basin-wide intensity over the western North Pacific: downscaled CMIP5 projections. Adv Atmos Sci 32:613–623. https://doi.org/10.1007/s00376-014-4105-4
Weatherford CL, Gray WM (1988a) Typhoon structure as revealed by aircraft reconnaissance. Part I: Data analysis and climatology. Mon Wea Rev 116:1032–1043. https://doi.org/10.1175/1520-0493(1988)116,1032:TSARBA.2.0.CO;2
Weatherford CL, Gray WM (1988b) Typhoon structure as revealed by aircraft reconnaissance. Part II: structural variability. Mon Wea Rev 116:1044–1056. https://doi.org/10.1175/1520-0493(1988)116,1044:TSARBA.2.0.CO;2
Webster PJ, Holland GJ, Curry JA, Chang HR (2005) Changes in tropical cyclone number, duration and intensity in a warm environment. Science 309:1844–1846. https://doi.org/10.1126/science.1116448
Wu C-C (2013) Typhoon Morakot (2009): Key findings from the Journal TAO for improving prediction of extreme rains at landfall. Bull Amer Meteor Soc 94:155–160. https://doi.org/10.1175/BAMS-D-11-00155.1
Wu L, Zhao H (2012) Dynamically derived tropical cyclone intensity changes over the western North Pacific. J Clim 25:89–98. https://doi.org/10.1175/2011JCLI4139.1
Wu L, Wang B, Geng S (2005) Growing typhoon influence on East Asia. Geophys Res Lett 32:L18703. https://doi.org/10.1029/2005GL022937
Xu J, Wang Y (2010a) Sensitivity of tropical cyclone inner-core size and intensity to the radial distribution of surface entropy flux. J Atmos Sci 67:1831–1852. https://doi.org/10.1175/2010JAS3387.1
Xu J, Wang Y (2010b) Sensitivity of the simulated tropical cyclone inner-core size to initial vortex size. Mon Wea Rev 138:4135–4157. https://doi.org/10.1175/2010MWR3335.1
Yen T-H, Wu C-C, Lien G-Y (2011) Rainfall simulations of typhoon Morakot with controlled translation speed based on EnKF data assimilation. Terr Atmos Ocean Sci 22(6):647–660. https://doi.org/10.3319/TAO.2011.07.05.01
Yohei, Yamada Masaki, Satoh Masato, Sugi Chihiro, Kodama Akira T., Noda Masuo, Nakano Tomoe, Nasuno (2017) Response of Tropical Cyclone Activity and Structure to Global Warming in a High-Resolution Global Nonhydrostatic Model. J Clim 30(23):9703–9724. https://doi.org/10.1175/JCLI-D-17-0068.1
Yoshimura J, Sugi M (2005) Tropical cyclone climatology in a high-resolution AGCM—impacts of SST warming and CO2 increase. SOLA 1:133–136. https://doi.org/10.2151/sola.2005-035
Yuan J, Wang D, Wan Q, Liu C (2007) A 28-year climatological analysis of size parameters for northwestern Pacific tropical cyclones. Adv Atmos Sci 24:24–34. https://doi.org/10.1007/s00376-007-0024-y
Zhang F, Tao D (2013) Effects of vertical wind shear on the predictability of tropical cyclones. J Atmos Sci 70:975–983. https://doi.org/10.1175/JAS-D-12-0133.1
Zhao X, Li J (2009) Possible causes for the persistence barrier of SSTA in the South China Sea and the vicinity of Indonesia. Adv Atmos Sci 26:1125–1136. https://doi.org/10.1007/s00376-009-8165-9

Publisher's Note